Modelling of the thermodynamic and solvation properties of electrolyte solutions with the statistical associating fluid theory for potentials of variable range

Jens M. A. Schreckenberg*, Simon Dufal*, Andrew J. Haslam*, Claire S. Adjiman*, George Jackson*, Amparo Galindo**

[a] *Qatar Carbonates and Carbon Storage Research Centre, Department of Chemical Engineering, Imperial College London, South Kensington Campus, London SW7 2AZ, UK.*

Abstract

An improved formulation of the extension of the statistical associating fluid theory for potentials of variable range to electrolytes (SAFT-VRE) is presented, which incorporates a representation for the dielectric constant of the solution that takes into account the temperature, density and composition of the solvent. The proposed approach provides an excellent correlation of the dielectric-constant data available for a number of solvents including water, representative alcohols and carbon dioxide, and it is shown that the methodology can be used to treat multi-solvent electrolyte solutions. Models for strong electrolytes of the metal-halide family are considered here. The salts are treated as fully dissociated and ion-specific interaction parameters are presented. Vapour-pressure, density, and mean ionic coefficient data are used to determine the ion-ion and solvent-ion parameters and multi-salt electrolyte solutions (brines) are then treated predictively. We find that the resulting intermolecular potential models follow physical trends in terms of energies and ion sizes with a close relationship observed with well-established ionic diameters. A good description is obtained for the densities, mean-ionic activity coefficients, and vapour pressures of the electrolyte solutions studied. The theory is also seen to provide excellent predictions of the osmotic coefficient and of the depression of freezing temperature and provides a qualitative estimate of the solvation free energy. The vapour pressure of aqueous brines is predicted accurately, as is the density of these solutions, although not at the highest pressures considered. Model parameters and calculations for the vapour-liquid and liquid-liquid equilibria of salts in water+methanol and water+n-butan-1-ol are presented. In addition, it is shown that the salting-out of carbon dioxide in sodium chloride solutions is captured well using a predictive model.

Keywords: SAFT-VR, Equation of state, Phase behaviour, Water, Electrolyte, Alcohols, Solvation energy

*Current address:Shell Global Solutions, International BV Shell Technology Center Amsterdam, Grasweg 31 NL -1031 HW, Amsterdam, The Netherlands

**Corresponding author

Email address: a.galindo@imperial.ac.uk (Amparo Galindo)

1. Introduction

Electrolyte solutions are ubiquitous in the natural world and, accordingly, of fundamental interest in chemical, biological, geological and industrial systems. Of course, electrolytes in nature rarely occur as solutions of salt in pure water; the salt (or salts) will be commonly present in aqueous systems involving other species. When salts are added to simple (non-electrolyte) solutions, the thermodynamic properties of these solutions may be substantially altered, leading, for example, to an increase in the boiling temperature, a reduction in the vapour pressure, a variation in the density, and so-called salting-in and out effects. Knowledge of such properties may be crucial in the design and understanding of chemical processes; an ability to model electrolytes is thus of importance.

Modelling electrolyte solutions predictively at the molecular level presents a considerable challenge, as both short-range repulsive and attractive (dispersion and often hydrogen-bonding), and long-range polar and Coulombic interactions all need to be taken into account. In developing equations of state to study the thermodynamic properties of electrolyte solutions, the short-ranged forces can be accounted for with common non-electrolyte activity coefficient g^E models, such as the Wilson approach [1], NRTL [2] or UNIQUAC [3], or by using a (non-electrolyte) equation of state (EOS) such as the Peng-Robinson (PR) [4], Redlich-Kwong (RK) [5] or the statistical associating fluid theory (SAFT) [6, 7] approaches. Coulombic effects are usually incorporated using the seminal expressions for the primitive (solvent-averaged) models of Debye and Hückel [8, 9], or the mean spherical approximation (MSA) [10, 11] most frequently for the primitive model (PM), assuming either a restricted model for the ions (a model in which all the charges are taken to be of identical size) or an unrestricted one (in which each ion is represented with a specific diameter). By contrast, when using non-electrolyte EOSs to treat mixtures, one generally considers explicitly all of the species present, including the solvent, in an explicit manner. As a consequence of the adoption of PMs to treat electrolyte solutions in combination with non-electrolyte EOSs, the conversion between the Lewis-Randall (LR) (solvent-explicit) and McMillan-Mayer (MM) (solvent-implicit) frameworks needs to be considered. Pressure-explicit EOSs provide a straightforward relation to the LR framework, where the temperature T, pressure P and number of molecules N are the independent variables, while PMs for electrolytes are more naturally derived in the McMillan-Mayer framework, where the temperature T, the volume V, the chemical potential of the solvent μ_{solvent} and the number of salt molecules N_{salt} are the independent variables [12]. Haynes and Newman [12] noted that a correction term needs to be incorporated to account for the transformation of the free energy obtained in the MM framework, to the solvent explicit LR framework. The resulting contribution has, however, been shown to play little part in the calculated thermodynamic properties of solutions of 1:1 electrolytes at 25° C [13], and is often not considered.

There is a large body of work where different combinations of an electrolyte theory with an EOS is proposed; for a recent review, see Ref. [14]. Maribo-Mogensen *et al.* [15] have demonstrated recently that the performance of the DH and MSA representations of the electrostatics are quite similar within an EOS treatment, so that either approach may be adopted. The non-electrostatic contribution can be represented at the level of a cubic EOS; representative examples of this type of approach include the work of Fürst and Renon [16], who employed the EOS of Schwartzentruber [17] (a volume-corrected version of the Soave-Redlich-Kwong (SRK) [18] EOS) in combination with MSA-PM, and that of Myers *et al.* [13] or that of Macias-Salinas *et al.* [19], who used the PR EOS also with the MSA-PM. In order to obtain more-accurate properties of water, free-energy contributions due to hydrogen bonding (association) have also been incorporated in these methods. Lin *et al.* [20] examined the performance of both the PR and SRK EOSs, both in their original form and in the cubic-plus-association (CPA) extensions [14, 21], in which an association contribution from the theory of Wertheim [22–25] is included. Other examples of the use of the CPA EOS include the work of Wu and Prausnitz [26] and of Inchekel *et. al* [27]. Approaches based on more sophisticated perturbation theories have been increasingly employed: Jin and Donohue [28] used the perturbed anisotropic chain theory (PACT) [29, 30] in combination with a classic electrostatic free-energy term, and later Economou *et al.* [31] used the associating perturbed anisotropic chain theory (APACT) [32, 33] to treat solutions of strong electrolytes.

The first study in which electrolyte fluids were modelled within the statistical associating fluid theory (SAFT) perturbation approach was by Liu *et al.* [34], who combined the original SAFT EOS with the MSA-PM incorporating ion-dipole and dipole-dipole terms, following the work of Henderson *et al.* [35]. The SAFT-VR approach for components with Coulombic contributions, known as SAFT-VRE, was presented at about the same time; it has been employed with both square-well [36–38] and Yukawa [39, 40] potentials to represent the non-electrolyte interactions. Sadowski and co-workers [41–44] have developed an electrolyte version of PC-SAFT [45, 46], known as ePC-SAFT, by combining the DH theory with the PC-SAFT form of the free energy for the non-electrostatic terms.

The original SAFT-VRE and ePC-SAFT do not include an explicit treatment of the polar interactions. Long-range dipolar interactions have been considered explicitly in a large number of studies [47–53], and non-primitive SAFT models for electrolyte solutions in which the ion-dipole and dipole-dipole and the interactions are considered have also been presented [54–56]. Although the explicit treatment of long-range dipolar interactions is of interest it has also been shown in a Gibbs ensemble Monte Carlo simulation study [57] that there is no need to distinguish between short- and long-range interactions. For example, Sadus [58] has demonstrated that the fluid phase equilibria of the Stockmayer fluid (Lennard-Jones particles with point dipoles at their centre) with a moderately strong dipole moment (corresponding to that of water

or methanol in the vapour phase) is very similar to that of an equivalent Keesom [59] fluid in which only the average dispersive interactions are treated; one can conclude from this that both the orientational and energetic features of a dipolar fluid can be captured in an average fashion without explicitly accounting for the dipolar interactions. Moreover, Nezbeda [60] has shown that the long-range dipolar interactions play only a perturbative role in such systems. A detailed discussion of the range of applicability of the various approaches in temperature, pressure, vapour-liquid, liquid-liquid and solid-liquid equilibrium regions and on the adequacy of the methodologies for specific electrolyte solutions can be found in Refs. [14, 20, 61, 62].

The success of an accurate representation of electrolyte solutions depends intimately on the quality of the underlying solvent model, where water is usually the solvent under consideration. The focus of previous work carried out with SAFT-VRE [36–38] was almost exclusively on aqueous solutions (with the exception of the work in Ref. [38] where salting out in mixtures of water and *n*-alkanes was considered). An early SAFT-VR model of water was used in Refs. [36–38], which has subsequently been superseded by a more accurate one [63] that has been used successfully to describe the thermodynamics and phase equilibria of a variety of non-electrolyte aqueous mixtures [64–75]. It is clearly desirable that the SAFT-VRE methodology be updated to incorporate this improved model of water and to provide consistent models for the ionic species and the unlike interactions between the ions and solvent species, which is one of the goals of our current paper. The opportunity is also taken to incorporate further improvements within the SAFT-VRE framework. We propose an approach to incorporate a generic description of the dielectric constant of the solvents, which can be used to study mixed-solvent solutions. The predictive capability of the SAFT-VRE approach is maintained by using ion-specific models, accounting explicitly for the repulsive and attractive ion-solvent interactions. The development and use of ion-specific models allows one to study an arbitrary electrolyte system, even when no experimental solution data for the parent salt are available.

The explicit incorporation of electrostatic ion-solvent interactions in the theoretical treatment as, for example, in the work of Lui *et al.* [54], Zhao *et al.* [55], and Herzog *et al.* [56], leads naturally to an accurate description of solvation effects. On the other hand, when the polar interactions are treated implicitly, these solvation effects can be taken into account by the inclusion of a so-called Born contribution to the free energy. In contrast to previous work using SAFT-VRE, a Born contribution is incorporated in our current work; we demonstrate that this term is crucial to provide a physically reasonable prediction of the hydration free energies of the ionic species.

Within our detailed investigation and revised SAFT-VRE approach, we study a range of aqueous solutions of strong electrolytes of single and mixed salts considering a broad range of thermodynamic conditions and properties (saturation pressure, activity coefficient, density, osmotic coefficient, solvation energy, and

solution freezing point). We use aqueous mixtures of alcohols as test mixed-solvent systems to assess the capability of our methodology in representing the effect of added salts on the vapour-liquid and liquid-liquid phase equilibria.

2. Theory and thermodynamic relations

We consider salts C_{ν_+} A_{ν_-} which, in solution, fully dissociate according to

$$C_{\nu_{k,+}} A_{\nu_{k,-}} \rightarrow \nu_{k,+} C^{z_{k,+}} + \nu_{k,-} A^{z_{k,-}}, \tag{1}$$

where $\nu_{k,+/-}$ are the stoichiometric coefficients of the ions, while $z_{k,+}$ and $z_{k,-}$ are the charge of the cation and the anion, respectively. Since the salts are treated as fully dissociated, the total number of particles (solvent and free ions) is given by

$$N = \sum_{\text{solvent},\, j=1}^{n_{\text{solv}}} N_j + \sum_{\text{salt},\, k=1}^{n_{\text{salt}}} \nu_k N_k = \sum_{\text{solvent},\, j=1}^{n_{\text{solv}}} N_j + \sum_{\text{ions},\, l=1}^{n_{\text{ion}}} N_l, \tag{2}$$

where n_{solv}, n_{salt} and n_{ion} refer to the number of different types of solvents salts or ions present, respectively, and $\nu_k = \nu_{k,+} + \nu_{k,-}$ is the stoichiometric coefficient of salt k. The mole fraction x_i of species i is defined in the usual way as N_i/N, either for ions or solvents; in the case that i corresponds to an ion, the mole fraction can be obtained from the molality m_k of its parent salt k in solution using

$$x_i = \frac{\sum_{\text{salt},\, k=1}^{n_{\text{salt}}} \nu_{k,i} m_k}{\left(\sum_{\text{salt},\, k=1}^{n_{\text{salt}}} \nu_k m_k \right) + 1/\text{MW}_{\text{solv}}}, \tag{3}$$

where MW_{solv} represents the molecular mass of the solvent in (kg mol^{-1}).

In this implementation of the SAFT-VRE approach (see also [36, 37]), the free energy A of an electrolyte solution at a temperature T and volume V containing N particles, is written as a sum of six separate contributions:

$$A = A^{\text{Ideal}} + A^{\text{Mono}} + A^{\text{Chain}} + A^{\text{Assoc}} + A^{\text{Ion}} + A^{\text{Born}}. \tag{4}$$

The first four terms on the right hand side are those of the original SAFT-VR EOS [76, 77] for non-electrolytes and take into account the ideal (A^{Ideal}), segment-segment (A^{Mono}), chain formation (A^{Chain}) and association (A^{Assoc}) contributions to the free energy of the mixture. These four terms, together with the penultimate term (A^{Ion}), which accounts for the Coulombic interaction between the ions in the presence of solvent molecules, are equivalent to the previous formulation of SAFT-VRE [36, 37]. In our current paper

the procedure for the evaluation of the electrostatic contributions is refined, and an additional term (A^{Born}) is included to account for the free energy related to the process of charging the ionic species in solution. As no explicit treatment of the polar or ion-polar interactions is made, the Born term is used to incorporate the long-range electrostatic contribution of ion-solvent interactions, while the shorter range ion-solvent interactions are treated using square-well potentials of variable range, as are the shorter range solvent-solvent interactions. We also note here that the electrostatic contributions (A^{Ion} and A^{Born}) are considered at a primitive (solvent-implicit) level.

A schematic representation of the different contributions to the free energy of the SAFT-VRE EOS, taking the Born term into account, is presented in Figure 1. By separating the monomer term into the corresponding hard-sphere (repulsive) and dispersion (attractive) contributions,

$$A^{\mathrm{Mono}} = A^{\mathrm{HS}} + A^{\mathrm{Disp}}, \tag{5}$$

one can more-easily illustrate how the Born term contributes to the overall free energy. The Born term itself involves both charging and discharging contributions [78]:

$$A^{\mathrm{Born}} = A^{\mathrm{Disch.}} + A^{\mathrm{Charge}}. \tag{6}$$

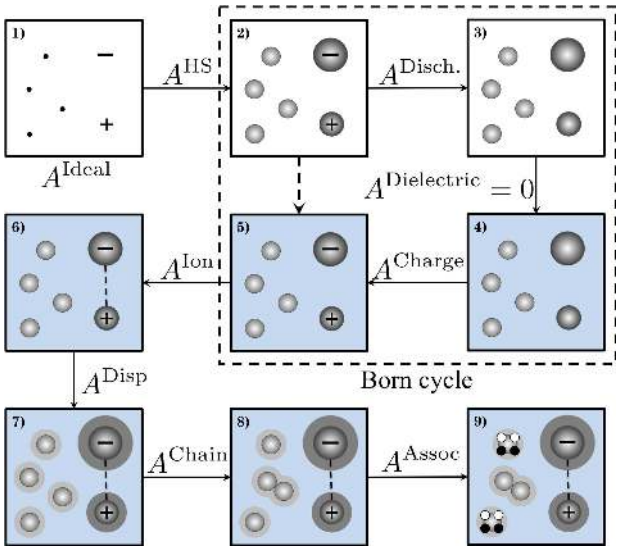

Figure 1: Schematic representation of the different contributions used in our current SAFT-VRE framework, equation (4). A^{Mono} is represented as the sum of A^{HS} and A^{Disp}, while $A^{\mathrm{Born}} = A^{\mathrm{Disch.}} + A^{\mathrm{Charge}}$. The shaded background in frames (4) to (9) represents the presence of a dielectric medium.

It is perhaps useful to note, as discussed in Ref. [13], that the reference system here corresponds to a perfect gas mixture of neutral and charged particles; this is represented in frame 1) of Figure 1. The use of this

reference is essential in order to allow for the calculation of the solvation free energies of ions in primitive models in which the solvent-ion electrostatic interactions are otherwise not included. In this perfect gas all interactions between particles are considered to be zero, and hence there is no contribution due to the electrostatic interaction between ions, but a self-energy term in vacuum is taken into account, as can be seen in the Born expressions given by equations (7) and (8). From frame (1), a perfect gas mixture with non-interacting charges in vacuum, the first step leads to a fluid of hard spheres with point charges, although in which the inter-particle Coulombic interactions are not yet taken into account(frame 2)); the free-energy contribution of this change is the purely repulsive hard-sphere contribution A^{HS}. In the second step the ions are discharged, leading to a mixture of hard spheres in vacuum (frame 3)); the contribution corresponding to this free-energy change is $A^{\mathrm{Discharge}}$. In the next step a continuous dielectric medium of dielectric constant D is introduced (schematically represented by the shaded background), leading to frame 4), a hard-sphere mixture in a dielectric medium. The free-energy change associated with this step is zero as there are no charges or multipoles interacting with the dielectric. Next, the ions are charged, leading to frame 5), a non-interacting charged-hard-sphere mixture in a dielectric medium, with a corresponding change in free energy A^{Charge}. Steps from 2) to 5) are known as the Born cycle. In frame 6) the Coulomb interactions between charges are taken into account (this is represented by the dashed line in the figure), and the corresponding system is a mixture of interacting charged hard spheres in a dielectric medium; the free-energy change is represented by A^{Ion}, which is treated here using the mean-spherical approximation (discussed in the following section). The last three steps illustrate the remaining contributions of the standard SAFT-VR EOS: the remaining part, A^{Disp}, of the monomer free energy is introduced in the change to frame 7) where dispersion interactions are taken into account; the formation of of molecular chains from the monomeric segments 8) and the inter-molecular association 9), with the corresponding free-energy contributions A^{Chain} and A^{Assoc}, respectively, complete the SAFT-VRE free energy. Frame 9), thereby, represents our full SAFT-VRE model representation of an electrolyte solution.

2.1. The Born solvation free energy

The Born solvation free energy, A^{Born}, can be defined as the change in free energy due to electrostatic interactions when ions are transferred from vacuum into a dielectric medium at infinite dilution. Assuming a primitive model, Born [78] considered the work required to transfer an ion from vacuum into a uniform dielectric medium of relative permittivity D, with the ion represented as a non-polarizable sphere of effective diameter σ_i, bearing a charge $z_i e$. In his original derivation a thermodynamic cycle is proposed in which the work of discharging the particle in vacuum and the work of recharging it in the medium are incorporated, while neglecting the work required to transfer the uncharged particle into the solvent. At infinite dilution

the final result leads to [78]

$$\mu_i^{\mathrm{Born}} = -\frac{e^2}{4\pi\epsilon_0}\left(1-\frac{1}{D}\right)\frac{z_i^2}{\sigma_i}, \tag{7}$$

for the chemical potential of an ion i in solution, where $\epsilon_0 = 8.854\times10^{-12}\mathrm{C}^2\mathrm{J}^{-1}\mathrm{m}^{-1}$ is the vacuum permittivity, and $e = 1.602\times10^{-19}$ C is the elementary charge. At constant volume and temperature, and assuming the same form of chemical potential for each of the ions, the Helmholtz free energy change is then given by

$$A^{\mathrm{Born}} = -\frac{e^2}{4\pi\epsilon_0}\left(1-\frac{1}{D}\right)\sum_{\text{ions } i}\frac{N_i z_i^2}{\sigma_i}. \tag{8}$$

A number of important phenomena related to the solvation of ions are neglected in developing this expression, but it nevertheless provides surprisingly good estimates of solvation energies, mostly due to the fact that the dominant contribution to the ion solvation is made by the electrostatic interaction of the ions and their polarised solvent environment. An excellent account of the approximations, and a discussion of extended treatments is provided in [79].

Equation (8) is obtained from equation (7) by integration of the standard relation $\mu_i = (\partial A/\partial N_i)_{V,T,N_{j\neq i}}$, whereby one is implicitly assuming that the dielectric constant is independent of V or N_j. For a more-realistic treatment, one might wish to account for the density (or compositional) dependence of the dielectric constant. In approaches where the relative permittivity is treated as constant, or as depending only on temperature the Born contribution to the chemical potential of an ionic species as given in equation (7) is recovered by differentiation of equation (8). There is no Born contribution to the chemical potential for a solvent species (with $z_i = 0$) and the corresponding contribution to the pressure (obtained via $P = -(\partial A/\partial V)_{N,T}$) is also zero:

$$P^{\mathrm{Born}} = 0. \tag{9}$$

If, however, a treatment is proposed wherein one incorporates the density and compositional dependence of the dielectric constant, differentiation of equation (8) with respect to the number of species of a given type results in the following expression for the Born contribution to the chemical potential:

$$\mu_i^{\mathrm{Born}} = -\frac{e^2}{4\pi\epsilon_0}\left[\left(1-\frac{1}{D}\right)\left(\frac{z_i^2}{\sigma_i}\right)+\frac{1}{D^2}\left(\frac{\partial D}{\partial N_i}\right)_{V,T,N_{j\neq i}}\sum_{\text{ions } i}\frac{N_i z_i^2}{\sigma_i}\right]. \tag{10}$$

The charging process associated with the MSA theory [10, 80] requires that

$$\left(\frac{\partial D}{\partial N_i}\right)_{V,T,N_{j\neq i}} = 0 \;\; \forall i \in (z_i \neq 0), \tag{11}$$

so that models proposed in the literature to treat the dielectric constant are usually not functions of the concentration of ions, *e.g.*, [81–83]), and it is notable that although the solvent does not carry a charge

($z_i = 0$ for a solvent species) a non-zero Born contribution for its chemical potential is obtained from equation (10). The corresponding pressure contribution in such a model is given by

$$P^{\mathrm{Born}} = \frac{e^2}{4\pi\epsilon_0} \sum_{\text{ions } i} \frac{N_i z_i^2}{\sigma_i} \frac{1}{D^2} \left(\frac{\partial D}{\partial V}\right)_{N,T}. \tag{12}$$

Our proposed model for the dielectric constant is discussed in detail in section 3.

2.2. The mean spherical approximation

The ionic contribution to the free energy used here represents the replacement of the solvent by a dielectric medium in which Coulombic interactions are screened. We use the mean-spherical-approximation (MSA) expressions within the primitive model, so that

$$A^{\mathrm{Ion}} = A^{\mathrm{MSA}}. \tag{13}$$

The MSA for symmetric (restricted) hard-sphere electrolytes within a primitive model treatment (implicit solvent) was first described by Waisman and Lebowitz [84]. Blum and Høye [10, 11] later extended the approach for asymmetric (unrestricted) hard-sphere electrolytes (MSA-PM); the internal energy in the MSA-PM model is given by

$$U^{\mathrm{MSA}} = -\frac{e^2 V}{(4\pi\epsilon_0) D} \left[\frac{\Gamma}{V} \sum_{\text{ions } i} \left(\frac{N_i z_i^2}{1+\Gamma\sigma_i}\right) + \frac{\pi}{2\Delta} \Omega P_n^2\right]. \tag{14}$$

Using the standard thermodynamic relation

$$U = \left(\frac{\partial(A/T)}{\partial(1/T)}\right)_{T,V,N}, \tag{15}$$

They show that the corresponding Helmholtz free energy can be written simply in terms of the internal energy U as (*cf.* reference [85])

$$A^{\mathrm{MSA}} = U^{\mathrm{MSA}} + \frac{\Gamma^3 k_{\mathrm{B}} T V}{3\pi}. \tag{16}$$

Hiroike [86] presented the same relation in an earlier paper, although it is important to note that there is a typographical error in equation (11) of the paper. The shielding parameter Γ is equivalent to the screening length κ obtained in the Debye-Hückel and restricted MSA approaches:

$$\Gamma^2 = \frac{\pi e^2}{(4\pi\epsilon_0) D k_{\mathrm{B}} T V} \sum_{\text{ions } i} N_i Q_i^2, \tag{17}$$

where k_B is the Boltzmann constant and Q_i is an effective charge given by

$$Q_i = \frac{z_i - \sigma_i^2 P_n(\pi/(2\Delta))}{1+\Gamma\sigma_i}. \tag{18}$$

The two parameters coupling the ion charge and size, P_n and Ω, are given by

$$P_n = \frac{1}{\Omega V} \sum_{\text{ions } i} \frac{N_i \sigma_i z_i}{1+\Gamma\sigma_i}, \tag{19}$$

and

$$\Omega = 1 + \frac{\pi}{2\Delta V} \sum_{\text{ions } i} \frac{N_i \sigma_i^3}{1 + \Gamma \sigma_i}, \tag{20}$$

while Δ relates to the free density (packing fraction) of the ions only:

$$\Delta = 1 - \frac{\pi}{6V} \sum_{\text{ions } i} N_i \sigma_i^3. \tag{21}$$

As a consequence of the highly coupled nature of the expressions the calculation of the shielding parameter Γ requires a numerical approach; here we use a Newton-Raphson method with an initial guess corresponding to half the Debye length, *i.e.*,

$$\Gamma_0 = \frac{\kappa}{2} = 0.5 \sqrt{\frac{e^2}{4D\epsilon_0 V k_\mathrm{B} T} \sum_i N_i z_i^2}\,; \tag{22}$$

satisfactory convergence is obtained after a maximum of six iterations [40, 87].

Other thermodynamic properties can be obtained from the standard relations by differentiation of the free energy. Blum and Rosenfeld [88] showed that derivatives of the Helmholtz free energy with respect to the shielding length Γ also correspond to

$$\left(\frac{\partial A^{\mathrm{MSA}}}{\partial \Gamma} \right)_{\Psi} = 0, \tag{23}$$

where Ψ represents any state variable.

With this in mind, an expression for the pressure is obtained as [85]

$$P^{\mathrm{MSA}} = -\frac{\Gamma^3 k_\mathrm{B} T}{3\pi} - \frac{e^2}{8\epsilon_0 D} \left(\frac{P_n}{\Delta} \right)^2, \tag{24}$$

for models where the dielectric constant is treated as independent of the volume and composition, and the corresponding chemical potential of species i is given by [85]

$$\mu_i^{\mathrm{MSA}} = -\frac{e^2}{(4\pi\varepsilon_0)D} \left\{ \frac{\Gamma z_i^2}{(1+\Gamma\sigma_i)} + \frac{\Omega \sigma_i^3}{12} \left(\frac{\pi P_n}{\Delta} \right)^2 + \frac{\pi^2 P_n^2 \sigma_i^3}{4\Delta^2} \left(\frac{1}{1+\Gamma\sigma_i} - \frac{1-\Omega}{3} \right) \right.$$
$$\left. + \frac{\pi P_n}{\Delta} \left[\frac{\sigma_i z_i}{(1+\Gamma\sigma_i)} - \frac{\pi P_n \sigma_i^3}{2\Delta} \left(\frac{1}{1+\Gamma\sigma_i} - \frac{1-\Omega}{3} \right) \right] \right\}. \tag{25}$$

When the dielectric constant depends on the volume or composition, the MSA expressions for the pressure and chemical potential incorporate additional terms resulting from the derivatives involved in the thermodynamic relations. The pressure is obtained by applying the chain rule:

$$\begin{aligned} P^{\mathrm{MSA}} = -\left(\frac{\partial A^{\mathrm{MSA}}}{\partial V} \right)_{T,N} &= -\left(\frac{\partial \tilde{A}^{\mathrm{MSA}}}{\partial V} \right)_{T,N,\Gamma,D} \\ &- \left(\frac{\partial \tilde{A}^{\mathrm{MSA}}}{\partial \Gamma} \right)_{T,N,V,D} \left[\left(\frac{\partial \Gamma}{\partial V} \right)_{T,N,D} + \left(\frac{\partial \Gamma}{\partial D} \right)_{T,N,V} \left(\frac{\partial D}{\partial V} \right)_{T,N} \right] \\ &- \left(\frac{\partial \tilde{A}^{\mathrm{MSA}}}{\partial D} \right)_{T,N,\Gamma} \left(\frac{\partial D}{\partial V} \right)_{T,N}, \end{aligned} \tag{26}$$

where $\tilde{A}^{\mathrm{MSA}}$ is the same free-energy function but where Γ and D are treated as independent variables. The second term in equation (26) is always zero (*cf.* equation (23)), while in the third term

$$\left(\frac{\partial \tilde{A}^{\mathrm{MSA}}}{\partial D}\right)_{T,N,\Gamma} = -\frac{U^{\mathrm{MSA}}}{D}, \tag{27}$$

and the derivative of the dielectric constant with respect to the volume may now be non-zero. Equivalent expressions are obtained for the calculation of other thermodynamic properties, such as the chemical potential of the species in solution. Derivatives of the dielectric constant with respect to the ionic species must be zero to satisfy the approximations used during the charging process in obtaining the free energy [11, 89], while in the case of the chemical potential of the solvent, a non-zero term may be obtained. As always, the fundamental thermodynamic relation between Helmholtz and Gibbs free energies must be satisfied.

2.3. Phase equilibria

The general solution of phase equilibrium between phases $\alpha, \beta, ...N_p$ requires equality of temperature, pressure, and chemical potential of each of the species i in the mixture,

$$T^{\alpha} = T^{\beta} = ... = T^{N_p}, \tag{28}$$

$$P^{\alpha} = P^{\beta} = ... = P^{N_p}, \tag{29}$$

$$\mu_i^{\alpha} = \mu_i^{\beta} = ... = \mu_i^{N_p} \quad \forall\, i, \tag{30}$$

and that the differences in chemical potentials of the ions between any given pair of phases are the same for all charged species when divided by the corresponding species charge [90]:

$$\begin{aligned}
&(\mu_j^{\alpha} - \mu_j^{\beta})/q_j = (\mu_k^{\alpha} - \mu_k^{\beta})/q_k \\
&\quad\vdots \\
&(\mu_j^{\alpha} - \mu_j^{N_P})/q_j = (\mu_k^{\alpha} - \mu_k^{N_P})/q_k \quad \forall j,k \in (z_j, z_k \neq 0)\,.
\end{aligned} \tag{31}$$

In our current work this constraint is applied to each pair of independent neutral species (salt) for the solutions with multiple salts [91]. These coexistence conditions are solved using a Levenberg-Marquardt [92, 93] algorithm, allowing the salt to be present in both the liquid and the vapour phase. In earlier work [36] the composition of the salt in the low-dielectric-constant phase (vapour phase in [36] or alkane-rich phase in [38]) was set to zero *a priori* and, as a result, the chemical potential difference of the salt ionic species did not need to be equated for the coexisting phases. The incorporation of a dielectric-constant expression that is density dependent in our current paper, together with the Born-term contribution to the free energy, naturally drive the salt into the water-rich liquid phase, and the phase-equilibrium problem is solved according to equations (28-31), with the chemical potential of the salt calculated and equated in both phases. The mole fraction of salt in the coexisting vapour phase is typically found to be of the order of 10^{-80}.

2.4. Activity and osmotic coefficients

In modelling electrolyte solutions it is especially useful to calculate the mean-activity coefficient (MAC) $\gamma_\pm$ of the ionic species (the salts) and the osmotic coefficient Φ of the solvent. There are a large amount of reliable experimental data for both properties (although mostly at ambient temperature, $T = 298$ K); these data for $\gamma_\pm$ and Φ provide a direct estimate of how accurately the chemical potential of the charged species and the solvent, respectively, are reproduced by the chosen approach.

The activity coefficient is obtained from the definition of the chemical potential of a species i in solution, which is given by

$$\mu_i(T, p, \mathbf{N}) = \mu_i^*(T, p, \mathbf{N}^*) + k_\mathrm{B}T \ln a_i(T, p, \mathbf{N}), \tag{32}$$

where μ_i^* is a reference chemical potential, corresponding to an infinitely dilute solution ($N_i \to 0$), $\mathbf{N}$ is the composition vector of the mixture, $a_i(T, p, \mathbf{N}) = x_i\gamma_i(T, p, \mathbf{N})$ is the activity, and γ_i the activity coefficient at the conditions of interest. The activity coefficient can also be related to the fugacity coefficients ϕ of the solution and the reference state by

$$\gamma_i(T, p, \mathbf{N}) = \frac{\phi_i(T, p, \mathbf{N})}{\phi_i^*(T, p, \mathbf{N}^*)}\,, \tag{33}$$

which at conditions corresponding to the reference state the activity coefficient takes a value of one by construction. The fugacity coefficient is easily obtained from the residual chemical potential $\mu^\mathrm{res} = \mu - \mu^\mathrm{Ideal}$, although a little care needs to be taken in the case of equations of state expressed in terms of volume as the independent variable instead of pressure; in this case the fugacity coefficient is obtained as

$$\phi_i(T, V_P, \mathbf{N}) = \frac{1}{Z} \exp\left(\frac{\mu_i^\mathrm{res}(T, V_P, \mathbf{N})}{k_\mathrm{B}T}\right), \tag{34}$$

where V_P denotes the volume corresponding to the specified pressure, and Z is the compressibility factor ($Z = PV_P/(Nk_\mathrm{B}T)$).

Although the activity coefficients of the individual ions in equation (33) are treated as independent, distinguishing experimentally between the individual contributions of the different ionic species to the total free energy is not straightforward. In principle, a small change in solute composition allows one to measure the change in Gibbs energy and hence to estimate the activity coefficient of the solute. If deviations from the ideal (or reference) state are shared equally between ions then they share an equal contribution to the activity coefficient. In the more likely case that non idealities are not equally shared, the contributions to the activity coefficient will be different. Alternatively, one could propose changing the composition of just one ion species, leaving the compositions of other counter ions constant, but the electroneutrality constraint

would then be violated. It is therefore commonly assumed that the single-ion activity coefficient cannot be measured directly. Instead a mean-activity coefficient (MAC) $\gamma_\pm$ is defined:

$$\gamma_\pm = \left[\gamma_+^{\nu_+}\gamma_-^{\nu_-}\right]^{1/\nu}. \tag{35}$$

As phase equilibrium in electrolyte solution requires the equality of the combined salt chemical potential, an equality of mean ionic coefficients can also be used directly to calculate phase coexistence.
The group of Vera [94] have proposed an interesting method to measure single-ion activity coefficients, which takes advantage of the fact that, for a given salt, there is a fixed ratio of anion and cation concentrations. The single-ion activity coefficients (SIAC) are measured experimentally using ion-selective electrodes that allow one to distinguish the contributions of the individual ions to the electromotive force. The possibility of experimentally measuring these SIAC and their validity is still the subject of some debate (see, for example, [95–97]). Published values of SIAC [98–100] are found to be quite scattered at high concentrations, which would be the region of interest, as the Debye-Hückel limiting law corresponds to low concentrations; accordingly, SIAC are not considered in this work.

As an additional point, we note that the preferred concentration scale for electrolyte solutions is the molality (moles of solute, in our case salt, per kilogram of solvent). The conversion of the activity coefficient from the mole-fraction scale to the molality scale is carried out taking into account that in the molality scale the reference chemical potential corresponds to the chemical potential of a hypothetical *ideal* solution of unit molality [13, 101, 102],

$$\gamma_i^m = \left(\frac{1}{1+\nu m MW_{\text{solv}}}\right)\gamma_i^x. \tag{36}$$

In our current work all of the activity coefficients are assessed in the molality scale γ_i^m. The superscript m indicating the molality is hence omitted hereafter.

The osmotic coefficient Φ is related to the chemical potential (and activity coefficient) of the solvent j in the solution. It can be determined from [13]

$$\Phi_j = -\frac{\ln\left(x_j\gamma_j\right)}{\nu\, m\, MW_{\text{solv}}}. \tag{37}$$

2.5. Free energy of solvation

The free energy of solvation of a given species i corresponds to the change in free energy as a result of transferring it from an ideal-gas state (here a mixture of charged and uncharged non-interacting particles) into the bulk solvent, *i.e.*, the work associated with this transfer. The free-energy change associated with the formation of a cavity in the solvent and with all of the solute (ion)-solvent interactions contributes to this

thermodynamic property. The incorporation of the Born-term contribution, which accounts for the electrostatic component of the solvent-ion interaction in the expression for the total free energy (equation (4)), is essential in order to obtain agreement (even qualitatively) for this property in approaches where primitive-model expressions for the ionic terms are used.

The free energy of solvation G_i^{Hyd} of species i is directly related to the residual chemical potential, or the fugacity coefficient, at infinite dilution. Following Myers *et al.* [13] this free energy is determined as

$$\frac{\Delta G_i^{\mathrm{s}}(T,P)}{Nk_{\mathrm{B}}T} = \ln\phi(T,P,N_i \to 0) + \ln(MW_{\mathrm{solv}}m^{\ominus}) + \ln(P/P^{\ominus}), \tag{38}$$

where the standard-state molality is $m^{\ominus}$ =1 mol/kg and the standard pressure is $P^{\ominus}$ =1 bar. The second and third terms appear as a result of converting between the mole-fraction and molality scales and of taking into account the difference in pressure between the state of interest and the reference pressure.

3. A model for the dielectric constant

In a treatment based on the primitive model, the accuracy of the Coulombic free-energy contributions (A^{Ion} and A^{Born}) is crucially dependent on accurate values for the dielectric constant that is employed instead of an explicit accounting of the solvent electrical properties. Although there are a number of rigorous methods to obtain the dielectric constant from intermolecular interactions [103, 104], these are not easy to implement, requiring additional adjustable parameters to treat real fluids accurately, and are very difficult to extend to mixed-solvent solutions [105]. Recently Maribo-Mogensen *et al.* [106, 107] presented a model for the dielectric constant based on the framework developed by Onsager [108], Kirkwood [109], and Fröhlich [110], for use in conjunction with the CPA [14, 21] EOS. Harvey and Prausnitz [83] suggested that there is a direct empirical relationship between the dielectric constant D and the density of the polar medium that can be represented by a simple relation that has also been shown to be transferable for a number of solvent mixtures [102]. Here we follow Uematsu and Franck [81], and propose a simple expression that takes into account the change in the dielectric constant with temperature and density of the solvent

$$D = 1 + \rho_{\mathrm{solv}}d\,, \tag{39}$$

where d is a solvent-dependent parameter, and $\rho_{\mathrm{solv}} = N_{\mathrm{solv}}/V$ is the number density of the solvent. Before presenting the final expression, it is useful to recall that a dielectric constant $D = D(T,V,\mathbf{N})$ that depends on temperature, volume and composition requires a consideration of the derivatives with respect to any of these variables so that the standard thermodynamic relation

$$G = \sum_i N_i\mu_i = A + PV \tag{40}$$

is be satisfied. The chemical potential and the pressure can both be expressed in terms of the Helmholtz free energy as described earlier. If the dielectric constant D is a function of density, *cf.* equation (39) , then equation (40) takes the following form:

$$\sum_{i=1}^{n} N_i \left[\left(\frac{\partial \tilde{A}}{\partial N_i} \right)_{T,V,N_{j\neq i},D} + \left(\frac{\partial \tilde{A}}{\partial D} \frac{\partial D}{\partial N_i} \right)_{T,V,N_{j\neq i}} \right] = A - V \left[\left(\frac{\partial \tilde{A}}{\partial V} \right)_{T,N,D} + \left(\frac{\partial \tilde{A}}{\partial D} \frac{\partial D}{\partial V} \right)_{T,N} \right] , \qquad (41)$$

where $\tilde{A}$ is the same free-energy function but where D is treated as an independent variable, and $n = n_{\text{ion}} + n_{\text{solv}}$ is the total number of species (ions and solvents). One route to ensure that the fundamental equation is recovered is to propose expressions for the dielectric constant that lead to the cancellation of the second term on the left-hand side with the third term on the right, *i.e.*,

$$\left(\frac{\partial D}{\partial V} \right)_{T,N} = -\frac{1}{V} \sum_{i=1}^{n} N_i \left(\frac{\partial D}{\partial N_i} \right)_{T,V,N_{j\neq i}} . \qquad (42)$$

The simple expression proposed in equation (39) fulfills this condition.

Extensive experimental data for the dielectric constant of water are available over wide ranges of temperature, pressure, and density [111]. In Figure 2, the experimental dielectric constant D_{exp} and density ρ_{exp} are combined to give an experimental parameter

$$d_{\text{exp}} = \frac{D_{\text{exp}} - 1}{\rho_{\text{exp}}}, \qquad (43)$$

which is represented in the figure as a function of the inverse temperature. As can be seen from Figure 2, the plotted points of d_{exp} collapse onto a single curve for a broad range of temperatures. This suggests that d_{exp} can be expressed as a simple temperature-dependent function. The deviations observed at higher temperatures can be explained by the fact that the dielectric constant at these conditions (low density) tends to its value in vacuum $D = 1$ and hence the numerator in equation (43) is more sensitive to the accuracy of the measured dielectric constant.

The direct proportionality observed for d_{exp} over a wide range of $1/T$ in Figure 2 suggests that a linear correlation is appropriate. An accurate description of the temperature-dependent parameter d for a pure component is thus obtained as

$$d = d_V \left(\frac{d_T}{T} - 1 \right), \qquad (44)$$

where d_V and d_T are component-specific parameters in units of dm^3/mol and K, respectively. This correlation performs very well within the temperature range indicated in Table 1. (Note that for $T > d_T$, the correlation leads to values of the dielectric constant that are less than one; its use is therefore strictly restricted to $T \leqslant d_T$). In the case of carbon dioxide the dielectric constant is found to be dependent on the density only, leading to d_T=0 and thus a negative value for d_V. In Figure 3 the proposed correlation for the density dependence of the dielectric constant of water at different temperatures is compared with the

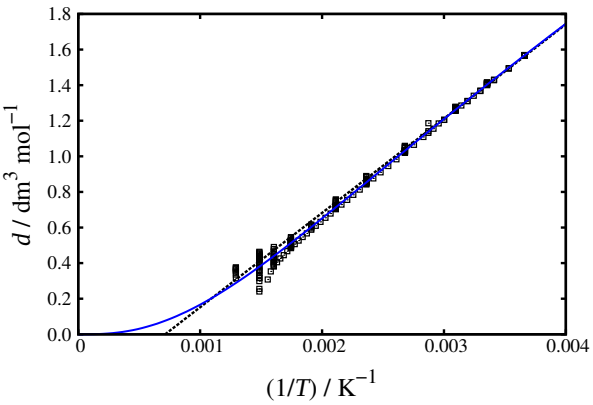

Figure 2: Ratio of the dielectric constant of water and the density, $d = (D-1)/\rho$, for a range of temperatures. The open squares correspond to experimental data [111]. A linear relation for d in terms of the inverse temperature is represented as the dashed line and an exponential form is represented as the continuous curve.

corresponding experimental data. The estimated parameter values for the model are reported in Table 1. An accurate representation of the experimental data can be achieved with this relation over the temperature range considered. The experimental dielectric constant of water is obtained with a percentage absolute average deviation (% AAD) of 0.97% for temperatures ranging between 273 and 423 K, and densities up to 63 mol / dm^3 (when considering data ranging from 273 to 773 K the % AAD is 5%).

This simple correlation for the dielectric constant has also been tested for other polar molecules. In Table 1 the estimated parameters are reported for selected alkanols and carbon dioxide. It is interesting to note that the proportionality of $1/d_V \sim d_T$ is maintained for all of the molecules considered in our study.

The applicability of the correlation to the temperature range $T < d_T$ does not cause particular problems in the context of the work presented here as only states at temperatures below d_T are considered. If higher temperatures are to be examined, a minor modification can be introduced by considering an exponential dependence:

$$d = \frac{d_V}{T}\left(1 - \exp\left(-\frac{d_T}{T}\right)\right)^2 . \tag{45}$$

The parameters of the exponential correlation for water obtained using equation (45) are also included in Table 1 (note that the units of d_V in this case are dm^3/(mol K)), and a comparison with experimental data and with the linear model can be seen in Figure 3.

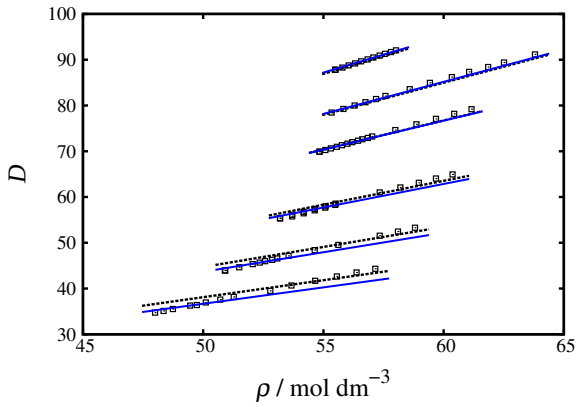

Figure 3: The dielectric constant of water at different densities and temperatures T = 273, 298, 323, 373, 423 and 473 K (the higher values of the dielectric constant represent the lower temperatures). The open squares represent the experimental data of Ref. [111]. The dashed curves correspond to the linear correlation, equation (44), and the continuous curves to the exponential correlation, equation (45).

In order to predict the dielectric constant of solvent mixtures, mixing and combining rules for the d parameter have to be considered. Following Harvey and Prausnitz [83], a van der Waals one-fluid mixing rule is used:

$$d(x_i^{'}) = \sum_i \sum_j x_i^{'} x_j^{'} d_{ij} \,, \tag{46}$$

where the prime denotes the use of salt-free mole fractions $x_i^{'} = N_i/(\sum_{\text{solvent},j} N_j)$, where i and j are solvent molecules , and d_{ii} corresponds to the parameter value of a pure component determined with equation (44). The unlike d_{ij} parameters are obtained using an arithmetic mean:

$$d_{ij} = \frac{d_{ii} + d_{jj}}{2}. \tag{47}$$

In Figure 4 the values of the dielectric constant determined with our procedure for a mixture of water and ethanol are compared with the corresponding experimental data at different temperatures, noting that in equation (39) the density of the mixture of water and ethanol is calculated using the SAFT-VR EOS. The SAFT-VR intermolecular model parameters used for this mixture are taken from previous work [63, 68]. As can be seen, the experimental dielectric constant of the mixture is described very accurately at all temperatures and compositions considered. The simplicity and transferability of the proposed treatment for a wide number of components and multi-component mixtures is quite remarkable. In the next section, this model of the dielectric constant is used in a study of the thermodynamic and solvation properties of a number of electrolyte solutions.

component	MW [g/mol]	d_V [dm^3/mol]	d_T [K]	% AAD	data points	Equation
water	18.02	0.3777	1403.0	0.97	100	44
water†	18.02	458.8†	923.6	0.69	100	45
methanol	32.05	0.5484	1011.0	0.86	36	44
ethanol	46.07	0.9480	732.1	1.44	30	44
propan-1-ol	60.10	1.269	641.7	0.44	8	44
propan-2-ol	60.10	1.667	550.1	1.08	18	44
n-butan-1-ol	74.12	1.515	593.3	1.13	14	44
n-butan-2-ol	74.12	2.555	461.6	1.06	4	44
t-butanol	74.12	2.616	417.1	3.74	23	44
n-pentan-1-ol	88.15	1.991	527.8	1.33	8	44
n-hexan-1-ol	102.17	2.860	457.1	1.46	3	44
carbon dioxide	44.01	−0.025	0.0	1.45	107	44

Table 1: Molecular weight and parameters for the correlations of the dielectric constant described by equations (44) and (45), and the corresponding percentage absolute average deviation (% AAD= $100/N_X \sum_{k=1}^{N_X} \left|X_k^{\rm exp} - X_k^{\rm calc}\right| / X_k^{\rm exp}$) from the experimental values for different polar solvents. † denotes the use of the exponential correlation of equation (45), in which case d_V is expressed in dm^3/(mol K).

4. Intermolecular potential models

We consider strong alkali-halide electrolytes including the Li^+, Na^+, K^+, Rb^+, F^-, Cl^-, Br^-, I^- ions, in water or mixed aqueous solvents. Electrolytes in pure water are considered first, using the 4-site associating square-well model of Clark *et al.* [63] to represent water. This model features a single square-well central core ($m_{s,i} = 1$) with four association sites, two of type 'H' and two of type 'e', incorporated to mediate hydrogen bonding; only 'H-e' bonding is allowed. (The values of the molecular parameters are included in Table 2 for completeness.) The effect of the addition of salts to mixed solvents is also examined; specifically, mixtures of water + methanol, water + *n*-butan-1-ol, and water + carbon dioxide are considered. Water + methanol mixtures are fully miscible in the liquid phase; this system provides a good test of the ability of the method to describe the effect of electrolytes on the vapour-liquid equilibrium of mixtures. Solutions in water + *n*-butan-1-ol and water + carbon dioxide are chosen as they are representative of mixtures which exhibit liquid-liquid separation, and where salting out effects may be observed. Furthermore, experimental data are available for each of these systems. Methanol and *n*-butan-1-ol are modelled as non-spherical molecules; we adopt a relation presented previously [63, 114, 115]

$$m_{s,i} = \frac{\mathrm{C} - 1}{3} + 1.2, \tag{48}$$

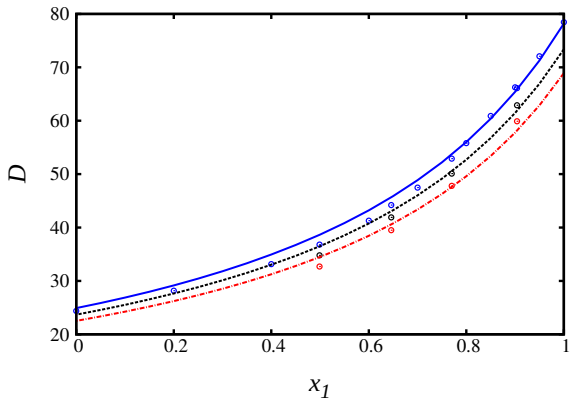

Figure 4: Dielectric constant for water (1) + ethanol (2) at a constant pressure of $P = 1$ bar and different temperatures. The curves represent calculations using the linear model for the dielectric constant, equation (44); the corresponding density at the given pressure and temperature is obtained using the SAFT-VR equation with the the models for water and ethanol developed in Refs. [63, 68]. The experimental data are represented by circles at (from bottom to top): $T = 298.15$ K, red; $T = 308.15$ K, black; $T = 318.15$ K, blue [111–113].

to determine the corresponding number of segments m_s, i to be used to represent each molecule, where C denotes the number of carbon atoms in the alcohol. Methanol is thus represented with $m_{s,i} = 1.2$ segments and n-butan-1-ol with $m_{s,i} = 2.2$ segments. The hydroxyl group (OH) of methanol is represented using three association sites: two of type 'e' and one of type 'H', which is consistent with the conclusions of Wolbach and Sandler [116] for the association scheme in alkanols from an assessment with molecular-orbital quantum-chemistry calculations. A further comparison of association schemes employed for water and for methanol in SAFT approaches can also be found in Ref. [14]. In the case of n-butan-1-ol the hydroxyl group (OH) is represented using only two association sites: one of type 'e' and one of type 'H'; the longer alkyl chain of this alcohol results is less self hydrogen bonding than in methanol in the pure compound. Carbon dioxide is modelled with two tangentially bonded segments $m_{s,i} = 2$ and is treated as non-associated. We use our previously presented model [53, 64, 65], which has been shown to provide a very good representation of the fluid phase behaviour of mixtures of carbon dioxide with water. The SAFT-VR parameter values for each of the pure solvents considered are summarised in Table 2.

The SAFT-VR unlike interaction parameter values for the aqueous solutions of methanol, n-butan-1-ol, and carbon dioxide are presented in Table 3. The arithmetic (Lorentz) combining rule is used to determine the unlike diameter,

$$\sigma_{ij} = \frac{\sigma_i + \sigma_j}{2} \ , \tag{49}$$

] interaction range,

$$\lambda_{ij} = \frac{\lambda_i \sigma_i + \lambda_j \sigma_j}{\sigma_i + \sigma_j} \ , \tag{50}$$

and the unlike bonding volume,

$$K_{ij} = \left(\frac{K_i^{1/3} + K_j^{1/3}}{2} \right)^3 \ , \tag{51}$$

parameters in all cases. The unlike dispersion and hydrogen-bonding energies, when required, are estimated by comparison to the appropriate experimental fluid-phase equilibrium data of the solvent systems, with no salt present. In the case of water + *n*-butan-1-ol, two additional association sites 'e*', which interact only with water molecules, are incorporated in the *n*-butan-1-ol model in order to obtain a good description of the phase separation in the liquid phase of the mixture [117]. A similar scheme was already used with a simplified version of SAFT [114] and was shown to be transferable to non-anionic surfactant solutions [115]. The final parameter values for water + *n*-butan-1-ol of this work are obtained by optimising the description of the experimental LLE data of the mixture at ambient conditions. The unlike intermolecular parameters used to model the fluid phase behaviour of water + carbon dioxide in this work are presented in Table 3; these parameters are adjusted to give the best representation of the solubility of carbon dioxide in water at the temperature of interest 323 K.

Molecule	$m_{s,i}$	σ_i / Å	λ_i	$(\varepsilon_i/k_\mathrm{B})$ / K	$r_{c,i}$/Å	$(\varepsilon_i^{hb}/k_\mathrm{B})$ / K
water	1.0	3.03420	1.78890	250.000	2.10822	1400.00
methanol	1.2	3.57163	1.79735	200.000	2.19477	2275.00
n-butan-1-ol	2.2	3.77610	1.80000	171.088	2.30489	3015.37
carbon dioxide	2.0	2.78640	1.51573	179.270	-	-

Table 2: Intermolecular SAFT-VR parameters for the square-well models of water [63], methanol [63], *n*-butan-1-ol [117], and carbon dioxide [118]: $m_{s,i}$ is the number of spherical segments constituting the chain molecule; σ_i is the diameter of the segment; λ_i is the range of the segment-segment square-well potential; ε_i is the depth of the segment-segment square-well potential; $r_{c,i}$ is the range of the site-site hydrogen-bonding square-well potential; and ε_i^{hb} is the depth of the hydrogen-bonding site-site square-well potential.

The salts are considered as fully dissociated and each of the ions is modelled as spherical ($m_{s,i} = 1$), with a hard-core diameter of σ_{ii}, carrying a single point charge (positive for cations or negative for anions). Coulombic and dispersion interactions between ions, and dispersion interactions between the ions and the solvent are taken into account. In our SAFT-VRE models the dispersion interactions are treated using square-well potentials of variable range λ_{ii} and well-depth ε_{ii} for ion-ion interactions, or range λ_{ij} and

Mixture	σ_{ij}	λ_{ij}	k_{ij}	$r_{c,ij}$/Å	$(\varepsilon_{ij}^{hb}/k_{\mathrm{B}})$ / K
water + methanol	3.30292	1.79347	0	2.15301	1784.66
water + *n*-butan-1-ol	3.40515	1.79505	−0.070	2.16547	1595.27
water + carbon dioxide	2.91030	1.65813	−0.058	-	-

Table 3: Unlike intermolecular SAFT-VR parameters for the square-well models of the aqueous mixtures of methanol [63], *n*-butan-1-ol and carbon dioxide where the unlike dispersion interaction is obtained from the correction to the Berthelot rule $\varepsilon_{ij} = (1 - k_{ij})\sqrt{\varepsilon_{ii}\varepsilon_{jj}}$.

well-depth ε_{ij} for ion-solvent interactions. As the salts have a negligible vapour pressure, the ion-ion and ion-solvent parameters are determined using mixture (solution) data directly in order to best represent the properties of the solutions. In previous work using SAFT-VRE [36–38] a number of the intermolecular parameters where determined *a priori*; in particular, Pauling ionic diameters for the corresponding crystals were used to characterise the ion sizes, and ion-ion dispersion interactions were not included. In our current work we consider a wide range of properties of the solutions and find that it is useful, in order to obtain quantitative agreement with experiment, to allow the effective ionic diameter to be different from that in the crystal, as done in other works (*e.g.*, see Refs. [13, 42]); we hence estimate the optimal values for the ionic diameters from a comparison to experimental data of single-salt aqueous solutions by minimisation of an objective function consisting of the relative difference between the calculated and experimental values of selected properties. Optimal values for the parameters are determined by minimizing a least-squares objective function using the Levenberg-Marquardt method [63, 68]:

$$\min F_{\mathrm{obj}} = \sum_i \frac{w_i}{n_{p,i}} \sum_j^{n_{p,i}} \left[\frac{X_{ij}^{\mathrm{calc}} - X_{ij}^{\mathrm{exp}}}{X_{ij}^{\mathrm{exp}}} \right]^2 , \tag{52}$$

where the superscripts "calc" and "exp" refer to calculated and experimental values, respectively, and w_i are the weights given to the experimental data sets of type i , each comprising $n_{p,i}$ data values. This function is well-behaved mathematically and is commonly used in this context, although it should be noted that a significant bias can arise when the data points span several orders of magnitude [63]. The properties considered in the optimisation are the vapour pressure, the density, and the mean activity coefficient at different temperatures. Following this procedure it is found that the range of the ion-ion square-well dispersion interaction always takes values close to 1.2; accordingly, we assign this value to the like and unlike ion-ion interactions as was done in previous work [36]. One should note that the absolute ranges of the ion-ion dispersion interaction still differ from each other since the range of attraction in real units is given by the product $\lambda_i\sigma_i$, so that the larger ions will have a greater range of the dispersion interaction than the smaller ions. The unlike ion-solvent diameters and square-well range parameters are obtained through the standard

combining rules given in equations (49) and (50).

The remaining like and unlike dispersion energy parameters (with the exception of the unlike ion-ion interactions) are estimated at the same time as the ionic diameters following the minimisation of the objective function, equation (52). It is possible to obtain a good estimate of the unlike ion-ion dispersion energy from the like ionic parameters using a procedure analogous to that proposed in reference [66], which is based on the work of Hudson and McCoubrey [119]. This method has already been employed to predict the value of k_{ij} in the correction to the Berthelot rule,

$$\varepsilon_{ij} = (1 - k_{ij})\sqrt{\varepsilon_{ii}\varepsilon_{jj}}, \tag{53}$$

based only on pure-component parameters, and has been shown provide a good model for the description of the fluid phase equilibria of a variety of mixtures [66]. Here we express the unlike ion-ion dispersion energy ε_{ij} as a function of the sizes of the ions, their polarisabilities α_0, and their ionisation potentials I, using equations (19) and (20) of reference [66] as:

$$\varepsilon_{ij} = \frac{3}{2}\frac{1}{\sigma_{ij}^6(\lambda_{ij}^3 - 1)}\frac{I_i I_j}{I_i + I_j}\frac{\alpha_{0,i}\alpha_{0,j}}{(4\pi\epsilon_0)^2}. \tag{54}$$

In the case of anions, the ionisation potential is estimated by the negative of the electron affinity of the neutral atom from which the anion is formed; for the (monovalent) cations, we use the second ionisation potential of the atom from which the cation is formed (or correspondingly higher-order ionisation potential for higher-valency ions). Polarisabilities and ionisation potentials are taken from Ref. [120] and shown in Table (4). The scheme for the determination of the complete ion-specific solution model is summarised in Table 5.

Table 4: Ionisation potentials and polarisability for the ions considered, taken from [120].

Ion	Li^+	Na^+	K^+	Rb^+	Ca^{2+}	F^-	Cl^-	Br^-	I^-
I/eV	75.64	47.29	31.63	27.29	50.91	3.40	3.61	3.36	3.06
α_0/ (10^{-24} cm^3)	0.03	0.18	0.83	1.40	0.47	1.04	3.66	4.77	7.10

5. Results

5.1. Aqueous solutions of single salts

We study first aqueous solution of the alkali halides formed from Li^+, Na^+, K^+, Rb^+, F^-, Cl^-, Br^- or I^-, excepting LiF, which is not considered due to its very low solubility and paucity of available experimental

Table 5: Summary of the proposed SAFT-VRE ion-specific interaction parameters for the models of electrolyte solutions. "Estimated" denotes that the parameters are obtained by optimisation of the objective function given in equation (52).

	σ_{ij}			λ_{ij}			ε_{ij}		
	Water	Cation	Anion	Water	Cation	Anion	Water	Cation	Anion
Water	Ref. [63]	Eq. (49)	Eq. (49)	Ref. [63]	Eq. (50)	Eq. (50)	Ref. [63]	Estimated	Estimated
Cation	-	Estimated	Eq. (49)	-	1.2	Eq. (50)	-	Estimated	Eq. (54)
Anion	-	-	Estimated	-	-	1.2	-	-	Estimated

data [42, 121] . Intermolecular potential model parameters for other ions can be easily determined at a later stage using these models as the counter ions (for example a model for Ca^{2+} can be obtained by using data for solutions of $CaCl_2$, $CaBr_2$, and CaI_2). We estimate the parameters by minimising the objective function given in equation (52). The experimental data chosen are the ones most-commonly found for simple electrolyte solutions: these include densities, mean-activity coefficients, and vapour pressures of the solutions, with weights of 1.0, 1.0 and 6.0, respectively. Data for the osmotic coefficient, the solvation free energy, and the depression of freezing point of the solvent are not used in the parameter estimation stage; they will be used later to assess the adequacy of the intermolecular potential models. The corresponding data are taken from literature, avoiding the temperature range close to the critical point of water ($T < 523$ K). Moreover, data for very concentrated brines are not taken into account. In concentrated solutions, the number of ions is so high that the assumption that the solvent can be treated as a continuous dielectric medium becomes difficult to justify; for example, in a 10 molal solution of a 1:1 electrolyte such as LiCl or NaCl in water, there are less than six solvent molecules per pair of ions so that, on average, the ions are separated by only one solvation shell of solvent molecules. Accordingly, we only consider systems up to a maximum salt concentration of 10 molal.

The development of ion-specific models as proposed here, is akin to the determination of group parameters in group-contribution approaches. The optimisation procedure may be carried out in two ways: sequentially or in a single iteration with all of the salt solutions considered together. In the first approach a reference salt, such as NaCl is chosen and its parameters are determined, which are then transferred to other salts containing Na^+ or Cl^-, and subsequent counterions are then considered. This methodology yield models which provide a very good representation of the thermodynamic properties for the reference salt, but the transferability of the individual ion parameters may be unoptimal: six parameters are estimated based on

the properties of the reference-salt system, resulting in a very good description of that particular salt but not necessarily of the individual ions. We opt to proceed with the second methodology, whereby one estimates parameters for all of the salts simultaneously. This results in a much more complicated parameter space, as there are many more parameters to estimate at the same time, however, the advantage of this method is that it provides greater consistency in the resulting models; the quality of the models for the different salts will be much closer than with a sequential estimation procedure. As this optimization is quite complex, with a total of 24 parameters to estimate for the chosen salts using over 2000 data points, we use multiple estimations with different starting points, allowing a broad coverage of the parameter space. The final set of intermolecular model parameters for the ions is chosen not only based on the quality of the description of the thermodynamic properties included in the estimation, but also ensuring that the resulting parameters take physically reasonable values, following accepted physical trends. The final SAFT-VRE intermolecular parameters for the ions considered in our current work are presented in Table 6, and the corresponding %AAD for the properties included in the estimation are given in Table 7.

Table 6: The SAFT-VRE intermolecular parameters for the models of the ions in aqueous solution. The ions are considered as spherical cores ($m_{s,\text{ion}}$=1.0), $\sigma_{\text{ion-ion}}$ is the hard-core diameter, while $\varepsilon_{\text{ion-ion}}$ and $\varepsilon_{\text{ion-water}}$ are the depths of the ion-ion and ion-water square-well potentials, respectively.

Ion	$\sigma_{\text{ion-ion}}$ / Å	$(\varepsilon_{\text{ion-ion}}/k_B)$ / K	$(\varepsilon_{\text{ion-water}}/k_B)$ / K
Li^+	1.5000	543.96	1002.1
Na^+	2.2021	1700.0	550.89
K^+	2.6385	926.04	413.54
Rb^+	3.2182	1541.4	493.34
F^-	1.9344	775.62	850.14
Cl^-	3.0794	831.39	420.38
Br^-	3.1666	523.95	387.94
I^-	3.5000	578.93	383.63

As can be seen from Table 6 our proposed models follow physically reasonable trends: the model ion diameters are such that they are seen to increase with atomic weight within a group, and each cation can be expected to be smaller than the corresponding anion in the same row of the periodic table. The sizes of the ion models are represented in Figure 5a, together with the Pauling [124] and Shannon [125] crystal diameters for comparison . Although the solvated diameters cannot be expected to be the same as those of

Table 7: % AAD of the vapour pressure (P_{sat}), density (ρ), and mean activity coefficient ($\gamma_{\pm}$) determined with the SAFT-VRE approach from the experimental data for the 15 alkali-halide salts studied [122, 123]. n_p corresponds to the number of experimental points, m_{max} to the maximum molality and T_{range} to the temperature range considered, respectively.

	% AAD					
Salt	P_{sat}	ρ	$\gamma_{\pm}$	n_p	m_{max}	T_{range}
LiCl	2.45	1.02	4.49	189	10	283–373 K
LiBr	2.75	3.24	4.63	463	10	283–353 K
LiI	2.83	1.94	6.16	81	7.6	293–348 K
NaF	0.93	0.24	3.15	50	1.0	293–473 K
NaCl	2.35	1.74	5.51	298	7.0	273–573 K
NaBr	1.75	0.65	3.63	154	9.5	283–368 K
NaI	3.1	1.3	4.49	101	9.7	276–363 K
KF	2.49	3.38	3.15	46	10	291–373 K
KCl	2.42	0.73	5.05	213	7.0	273–373 K
KBr	1.75	0.74	5.04	133	6.0	283–373 K
KI	2.06	2.35	2.97	116	9.0	278–423 K
RbF	1.72	2.5	4.81	56	9.0	288–323 K
RbCl	1.65	1	4.38	58	7.0	288–368 K
RbBr	1.62	0.34	1.68	59	5.0	291–323 K
RbI	1.35	1.54	1.9	46	5.6	291–298 K

the crystal it is reassuring to see that they follow similar trends.

It is not clear *a priori* how to judge what ranges of values of the dispersion energy for the interaction between like ions should be considered physically reasonable. However, it is highly desirable to be able to make such a judgement because one finds models of similar quality with dispersion energies differing over orders of magnitude. For ions of a given size the energies of like ion-ion dispersion can be compared to the corresponding values obtained from equation (54) (with $i = j$); this comparison is made in Figure 5c for the cations and in Figure 5d for the anions. Using the polarisability and ionisation potential of each ion, with a value of $\lambda_{ii} = 1.2$ for the range of the interaction corresponding to our models, the curves in Figures 5c and 5d represent the broad spread of values of the like dispersion energy parameter ε_{ii} that can be expected as a function of ionic diameter. It is clear from these plots that the variation of ε_{ii} that is observed during the parameter-estimation procedure is to be expected. Furthermore, it is interesting to find that the final dispersion-energy values obtained in the parameter estimation are close to those that would be obtained using equation (54), given the estimated ionic size.

It is also important to consider whether or not the values of the unlike water-ion dispersion interaction energies are physically reasonable, in view of the fact that the dipolar nature of the molecule is not treated explicitly in our proposed model of water; instead square-well potentials of variable range are used to describe the water-ion solvation interaction in an effective manner. In this regard, it is useful to examine the free energy of solvation. Our calculated free energies of solvation for the ions in aqueous solution are compared with experimental data of Fawcett [126] in Table 8. Although the average error is rather large ($\sim 35\%$), the qualitative agreement is good and, importantly, both the experimental and calculated values follow the same trends. As mentioned by Myers *et al.* [13], the inclusion of the Born term, which corresponds to the correct ideal-gas limit for a mixture of charged and uncharged particles, is essential in order to obtain physically relevant values of the solvation free energies in primitive models. In non-primitive models where the dipole of water (or the other polar solvents) is taken into account explicitly, better agreement with experiment can be obtained [56]; one should note, however, that in the latter work the models proposed are salt-specific, instead of ion-specific, so that different values for the solvation energy of a given ion are calculated depending on the parent salt. As our work is based on ion-specific models, the free energy of solvation of an ion is independent of the counter ion considered.

A clear relation between the calculated free energy of solvation and the water-ion dispersion energy parameter can be seen in Figure 5b. Note that the experimental solvation free-energy data are not used in the estimation of the model parameters (*i.e.*, the data are not considered in the objective function given in equation (52)). This agreement complements the qualitative agreement for the trends already noted between

the experimental and calculated solvation energies. The fact that the calculated solvation energies follow the experimental trend, and that this is mirrored in the trend of the intermolecular model parameter that is used to represent the complex ion-water interaction, provides a strong validation of the proposed model.

Table 8: Gibbs energy of solvation ΔG^{s} of the monovalent ions in aqueous solution: the experimental data reported by Fawcett [126] are compared with the corresponding values calculated with the SAFT-VRE approach.

Ion	$\Delta G^{\mathrm{s}}_{\mathrm{exp}}$ / (kJ/mol)	$\Delta G^{\mathrm{s}}_{\mathrm{SAFT-VRE}}$ / (kJ/mol)
Li^+	−529	−930
Na^+	−424	−618
K^+	−352	−504
Rb^+	−329	−418
F^-	−429	−723
Cl^-	−304	−429
Br^-	−278	−413
I^-	−243	−369

The performance of the SAFT-VRE approach with the models developed in our current work is illustrated in Figure 6 by comparison with experimental values of the properties included in the parameter-estimation procedure. One can discern that the theory provides a good description of the behaviour of the thermodynamic properties of the aqueous solutions of these monovalent salts. One could, of course, obtain an even better description using salt-specific (rather than ion-specific) models, however the slightly poorer accuracy is compensated by the superior predictive capability of ion-specific models, the use of ion-specific models enable the treatment of additional salts without any further parameter estimation, provided that the constituent ions have been studied previously, even in the case of salts for which no experimental data are available. It is also important to point out that there is no need for experimental data to estimate each unlike ion-ion interaction, since equation (54) is used to predict this parameter; this is especially useful in the case of brines composed of many ions for which experimental data may be unavailable.

Except for the vapour pressure, most of the available experimental measurements were made at ambient temperature, $T = 298$K; accordingly, less information on the temperature dependence of the other properties is included in the parameter-estimation procedure than would have been preferable. The dependence of the vapour pressure on the temperature is captured very well over a broad range of conditions, as shown in Figure 6c.

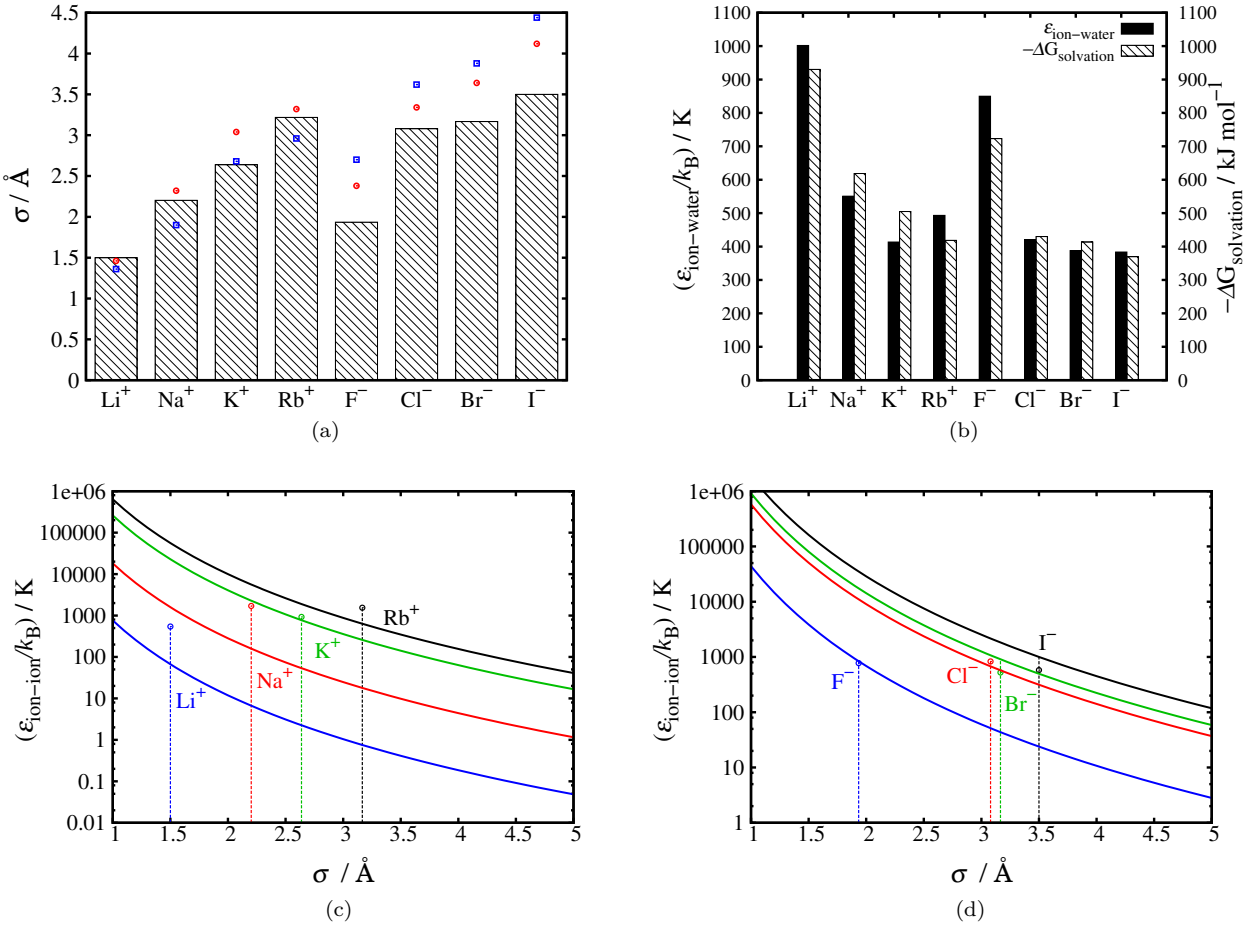

Figure 5: The SAFT-VRE intermolecular parameters for the ions in aqueous solution: (a) the estimated model ionic diameters (σ) are represented as the striped bars ; the blue squares indicate the Pauling [124] diameter values from the corresponding crystal structures, and the red circles those of Shannon [125].; (b) the ion-water dispersion energies (black bars), and the calculated Gibbs energy of solvation of the ions (striped bars); (c) and (d) the continuous curves represent the like ion-ion dispersion energies obtained using equation (54), as a function of the ionic diameter (the cations are presented in (c) and the anions in (d)), while the dashed lines indicate the estimated ionic diameters and the symbols the ion-ion dispersion energies estimated for each ion with the SAFT-VRE approach.

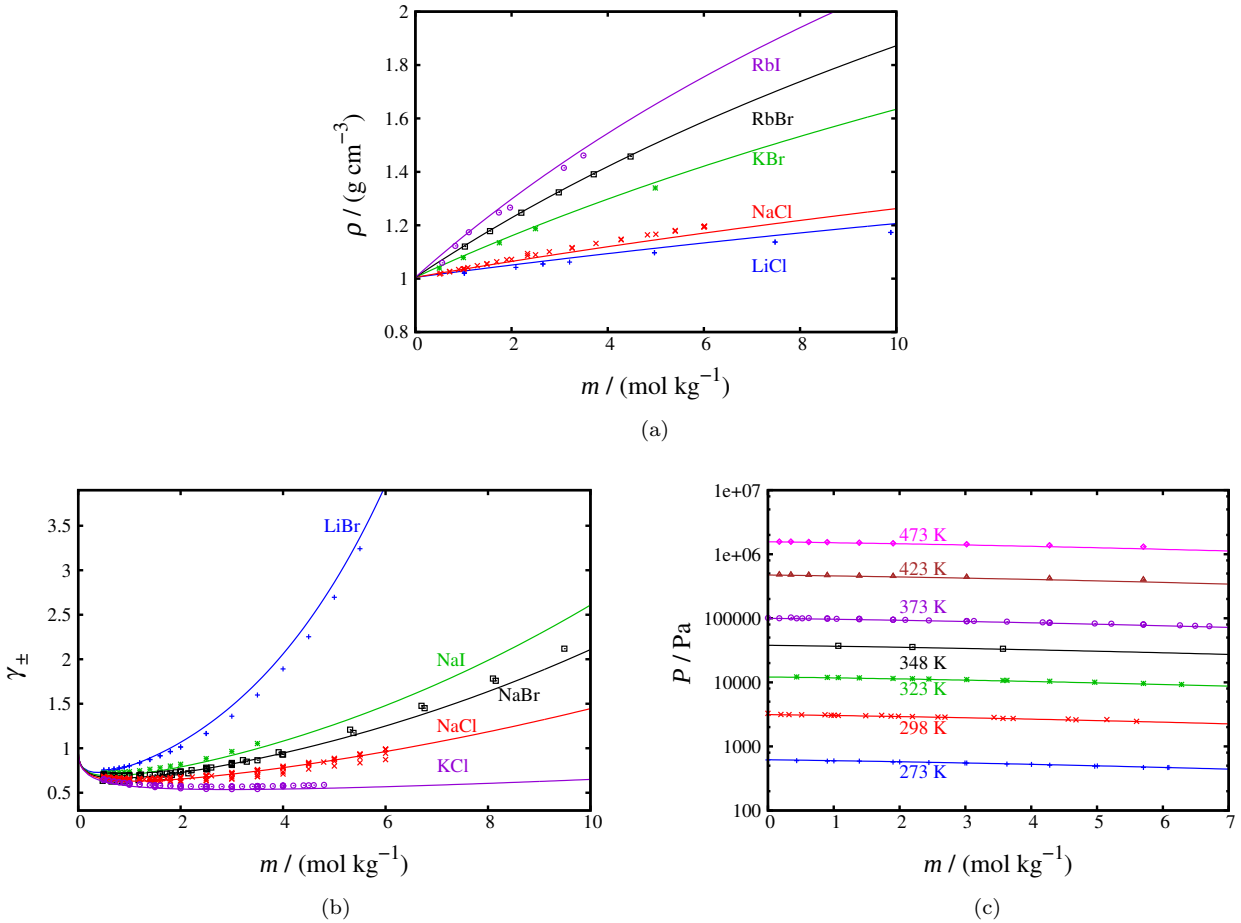

Figure 6: The dependence of the thermodynamic properties of aqueous solutions of monovalent alkali-halide salts on the molality m calculated with our SAFT-VRE approach compared with corresponding experimental data used in the parameter-estimation procedure: (a) densities ρ of the aqueous salts at a temperature of 298.15 K and a pressure of 1 bar; (b) mean-activity coefficients $\gamma_{\pm}$ of the aqueous salts at a temperature of 298.15 K and a pressure of 1 bar; (c) vapour pressures P of aqueous NaCl for a range of temperatures. In each case, the symbols represent the experimental data and the continuous curves the SAFT-VRE calculations.

5.2. Property prediction: osmotic coefficient; freezing-point depression; properties of multi-salt and multi-solvent brines

5.2.1. Osmotic coefficient

We now assess the capability of the models developed within our SAFT-VRE approach to predict properties that were not included for the determination of the intermolecular potential parameters. One of the properties of aqueous salts for which data are readily available is the osmotic coefficient Φ. As can be seen in Figure 7 and in Table 9 an excellent prediction of this property at ambient conditions (298 K and 1 bar) is obtained. The osmotic coefficient is related to the activity coefficient of the solvent (*cf.* equation (37)) and consequently to its chemical potential, so that an accurate representation of this property is important for phase equilibrium calculations.

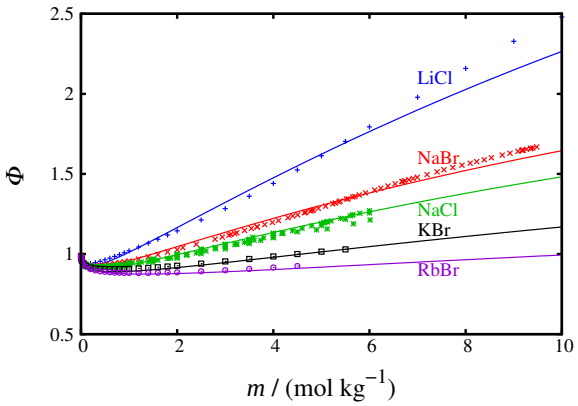

Figure 7: The dependence of the osmotic coefficient Φ on the molality m at a temperature of 298.15 K and pressure of 1 bar for aqueous solutions of monovalent alkali-halide salts compared with SAFT-VRE predictions. The symbols represent the experimental data [127–141] and the continuous curves the predictions with our SAFT-VRE approach.

5.2.2. Freezing-point depression

The depression in the freezing point of water upon the addition of salts can be determined from a knowledge of the activity coefficient of water as a function of the solution composition. Given the excellent agreement obtained in the prediction of the osmotic coefficient presented in the previous section, we now examine the experimental data for the depression of the freezing point when NaCl or LiCl are present in an aqueous solution. The analysis requires one to establish the conditions for phase equilibria at given pressure and temperature between a solid phase, assumed to be pure water, and a liquid phase containing the solvent (water in this case) and the solute (the salt in this instance) [149–151]. The dependence of the concentration

Table 9: Percentage average absolute deviation %AAD of the SAFT-VRE predictions from experimental data [127–148] for the osmotic coefficients of alkali-halide salts. n_p corresponds to the number of experimental points, m_{max} to the maximum molality and T_{range} to the temperature range considered, respectively.

Salt	% AAD(Φ)	n_p data	m_{max}	T_{range}
LiCl	2.77	83	10	298–373 K
LiBr	6.45	43	10	298 K
LiI	2.55	23	3	298 K
NaF	0.65	16	1	298 K
NaCl	1.55	201	7	288–573 K
NaBr	1.57	88	9.5	298 K
NaI	3.11	35	10	298 K
KF	2.8	41	10	298 K
KCl	1.24	119	5	273–373 K
KBr	2.59	98	5.5	298–373 K
KI	3.87	35	9	298 K
RbF	2.11	24	3.5	298 K
RbCl	2.26	32	7.8	298 K
RbBr	0.56	26	4.5	298 K
RbI	0.93	27	5	298 K

x_j of the solvent on the freezing temperature can be expressed as

$$\ln x_j = \left(\frac{T}{T_0} - 1\right) \frac{\Delta H^0_{\text{fus}}}{RT} - \frac{\Delta c^0_p}{R} \left(1 - \frac{T_0}{T} - \ln \frac{T}{T_0}\right) - \ln \gamma_j(p, T, \mathbf{N}). \tag{55}$$

where $T_0 = 273.15\ K$ is the normal freezing temperature of water, $\Delta H^0_{\text{fus}} = -6012.1$ J/mol is the heat of fusion of pure water, and the heat capacity difference between the solid and liquid phase (approximated as that for pure water) is assumed to be constant with temperature and equal to its value at T_0, $\Delta c^0_p = -38.12$ J/(mol K); these data of water are taken from [152]. As these constitute the only extra input (apart from the SAFT-VRE description of the activity coefficient of water γ_j), the methodology is predictive and quite straightforward to implement: for a given composition of the brine the temperature is changed until equation (55) is satisfied. The activity coefficient of water in the brine (γ_j) is calculated with the SAFT-VRE approach presented here. This provides a good test not only of our SAFT-VRE model of the various salts but also of the model of water, as it implicitly involves calculation of the properties of water under conditions at which pure water does not exist as a liquid, requiring that our model behaves correctly outside the range examined when the model was developed [63]. Results are illustrated in Figure 8, wherein it can be seen that our predictions provide a good representation of the experimental data [153–161] .

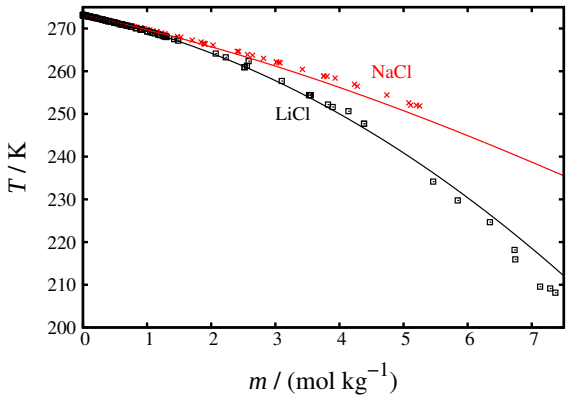

Figure 8: The depression of the freezing point of water upon addition of NaCl or LiCl. The symbols represent experimental data [153–161] and the continuous curves the calculations using equation (55) with the SAFT-VRE description of the activity coefficient of water for the salts solutions.

An approximation that might hamper the quality of our results is the assumption that the difference Δc^0_p in the heat capacity of solid and liquid water is constant with temperature. This approximation, albeit reasonable, becomes less satisfactory as the temperature decreases and its effect increases, which may help to explain why the accuracy deteriorates at higher molalities. Of course, the quality of the theoretical description of the aqueous electrolytes at the lowest temperatures may also deteriorate, since these temperatures lie further from the normal fluid range of pure water.

5.2.3. Multi-salt aqueous electrolyte solutions

As we have proposed models for the electrolyte solutions based on ion-specific intermolecular parameters, it is now straightforward to extend the method to study multi-salt brines. In order to treat such mixtures the unlike cation-cation (*e.g.*, Na^+ - K^+) and anion-anion (e.g., Cl^- - Br^-) interaction parameters (unlike ionic diameters, range and depth of the unlike square-well interaction), which have not been considered until this point, need to be determined. Our treatment is entirely predictive for these systems. We use the arithmetic rules presented earlier for the unlike ion diameter (equation (49)) and the range of the square-well interaction (equation (50)), and equation (54) is used to describe the unlike ion-ion dispersion energy. A comparison of experimental and predicted vapour pressures for various aqueous solutions of mixed salts at different temperatures is presented in Figure 9 . The predictions with our SAFT-VRE approach are found to be in excellent agreement with the available experimental data [162–164]. The corresponding densities of NaCl + KBr brine solutions at ambient conditions (298 K and 1bar) are displayed in Figure 10 for different total salt molalities. The SAFT-VRE predictions are found again to provide a very good representation of the experimental data. In Figures 11 (a) and (b) the densities of NaCl + KCl brines are displayed. These recent data cover a region of high pressure (0.92 to 68.42 MPa) and temperature (up to 397.97 K), far from those used in the estimation of the water model. As can be seen in the figures the predicted densities of pure water at these conditions are not as accurate as at lower pressure; this inadequacy of the SAFT-VR model of pure water accounts for a significant part of the inaccuracies observed in the prediction of the density of the brines. Although, as illustrated in Figures 11 (c) and (d) a noticeable improvement in the description of the density is observed when the SAFT-VRE predictions are adjusted to correct for the difference between the calculated and experimental pure-water densities, unfortunately deviations remain for the higher brine concentrations.

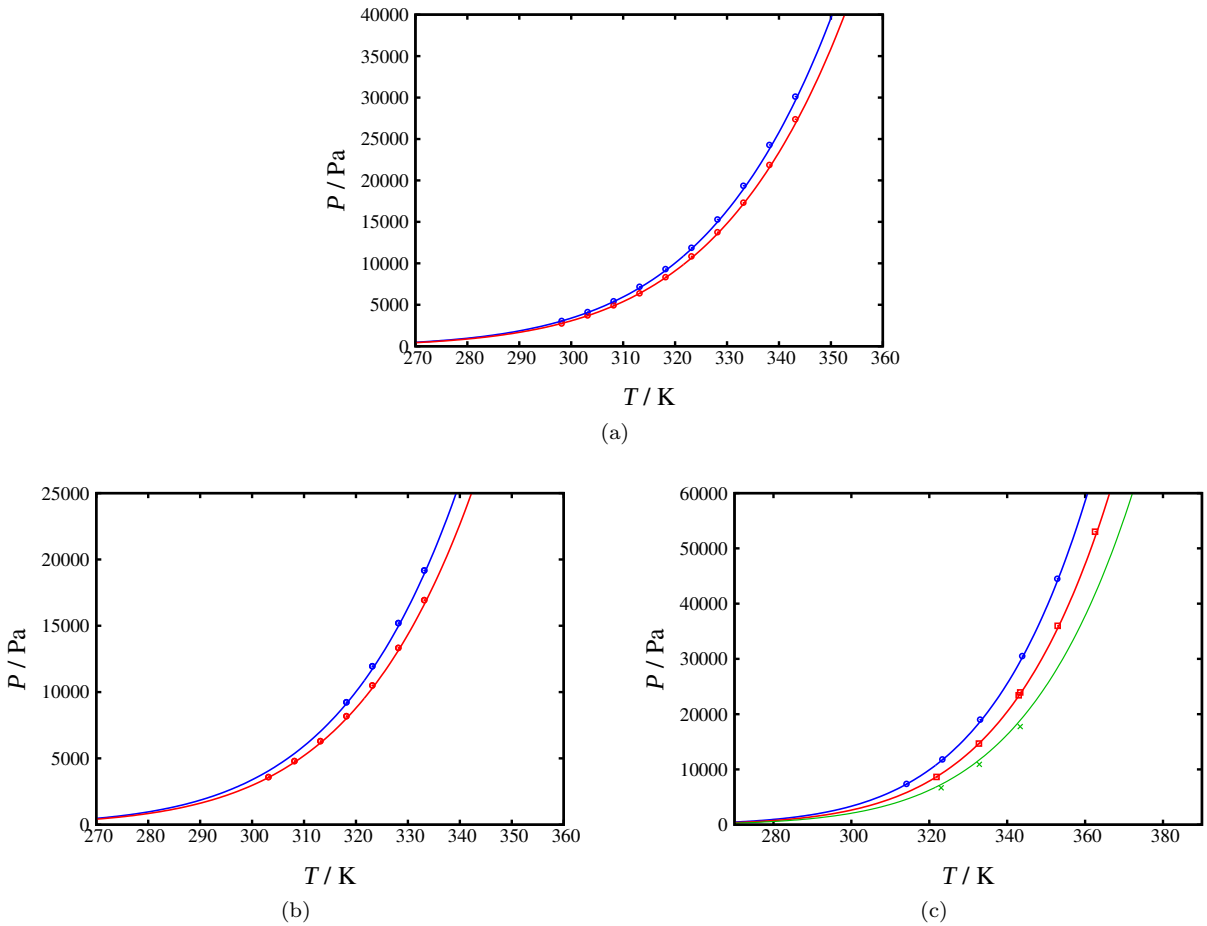

Figure 9: The temperature dependence of the vapour pressure for aqueous brine solutions of two different monovalent alkali-halide salts compared with the predictions of our SAFT-VRE approach. The corresponding concentrations of the brines are, in molality units: (a) 0.6 NaCl + 0.3 KCl (blue, top curve) and 2.0 NaCl + 1.3 KCl (red, bottom curve); (b) 0.5 NaCl + 0.5 KBr (blue, top curve) and 2.0 NaCl + 2.0 KBr (red, bottom curve); (c) 0.9 LiBr + 0.2 LiI (blue, top curve), 3.7 LiBr + 0.9 LiI (red, middle curve), and 5.6 LiBr + 1.4 LiI (green, bottom curve). The symbols represent the experimental data [162–164] and the continuous curves the SAFT-VRE predictions.

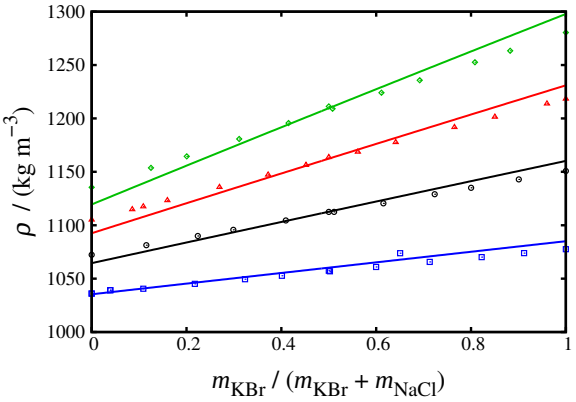

Figure 10: The density of aqueous brine solutions of NaCl + KBr as a function of the molality fraction of KBr at ambient condition (298.15 K and 1bar). Symbols represent experimental data [165–167] at different total salt molality ($m_{\mathrm{tot}} = m_{\mathrm{NaCl}} + m_{\mathrm{KBr}}$): 1 molal (blue squares); 2 molal (black circles); 3 molal (red triangles); and 4 molal (green diamonds). The continuous curves represent the predictions with the SAFT-VRE approach.

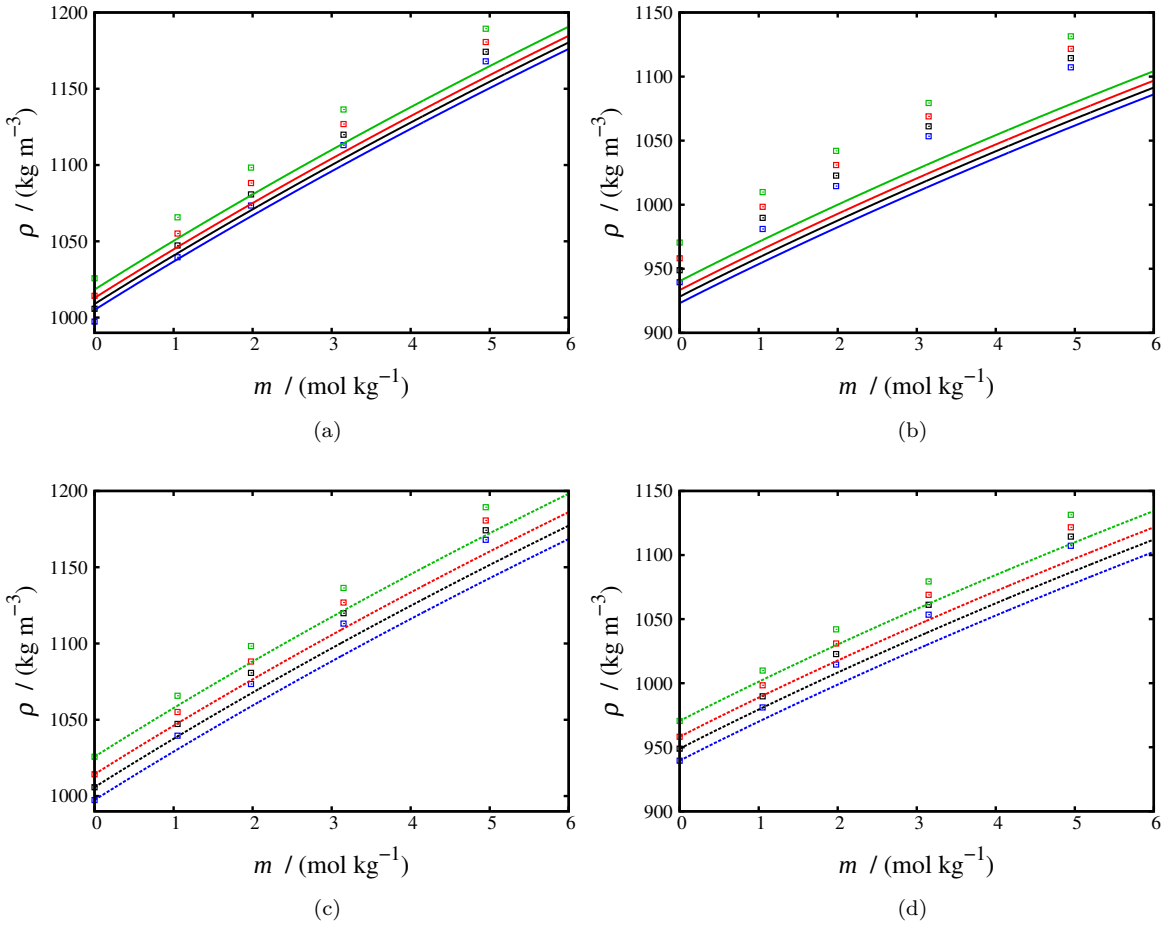

Figure 11: Isobaric density of aqueous brine solutions of NaCl + KCl as a function of total salt molality at a temperatures of (a) and (c) 298.12 K, and (b) and (d) 397.97 K. The symbols represent the experimental data [168, 169], the continuous curves in (a) and (b) the SAFT-VRE predictions at different pressures (from bottom to top: blue 0.92, black 19.92, red 39.92, and green 68.42 MPa), and the dashed curves in (c) and (d) the SAFT-VRE description corrected for the inaccuracy in the density of pure water.

5.2.4. Mixed-solvent brines

In addition to the treatment of brines containing more than one salt, our SAFT-VRE methodology can be used to investigate systems of more than one solvent. Here we focus on binary solvent systems containing methanol or *n*-butan-1-ol and water, using the models presented in Tables 2 and 3. To study the aqueous electrolyte solutions described in section 5.1 it was necessary to determine the water-ion unlike dispersion energy. In analogous fashion, the ion-alcohol unlike dispersion energy parameters need to be estimated in order to describe these mixed solvent systems; the unlike ion-alcohol hard-core diameter and interaction range are given by equations (49) and (50). As the data available for alcohol + salt systems is rather scarce we choose instead, for the ions considered, to adjust this dispersion energy to water + alkanol + salt fluid-phase equilibrium data of the mixed solvent systems directly.

Although the water + alkanol + salt mixtures are interesting systems, there are few models available [170–172]. In Figure 12 the SAFT-VRE calculations of the vapour-liquid equilibria are presented for methanol + water + salt ternary systems at atmospheric pressure for four salts, using estimated values of the methanol-ion dispersion energy parameter $\varepsilon_{\mathrm{Methanol-ion}}$, which are given in Table 10; the phase diagram of the water + methanol mixture is also included for reference so that the effect of adding salt can be discerned. The molalities indicated are those with respect to water, rather than for the combined solvent of water and methanol, *i.e.*, the mixture can be regarded as pure methanol added to an *m*-molal aqueous solution of salt. It is clear from the figure that the effect of the salts on the VLE of water-methanol is captured well with our approach. As expected the addition of salt leads to an increase in the boiling temperature of water; no such increase is seen in the boiling temperature of the mixture at the pure-methanol limit, as there is no salt present at this point. In general, at a given temperature the mole fraction of methanol in the vapour phase increases upon addition of salt, while that in the liquid phase decreases, as corresponds to a salting-out of methanol from the liquid.

Table 10: The unlike dispersion energy parameter $\varepsilon_{\mathrm{Methanol-ion}}$ between the ion and methanol estimated from the methanol-water-salt vapour-liquid equilibrium data at atmospheric pressure with the SAFT-VRE approach.

Ion	Li^+	Na^+	K^+	F^-	Cl^-	Br^-
$(\varepsilon_{\mathrm{Methanol-ion}}/k_{\mathrm{B}})$ / K	900.0	551.0	100.0	870.0	420.0	180.0

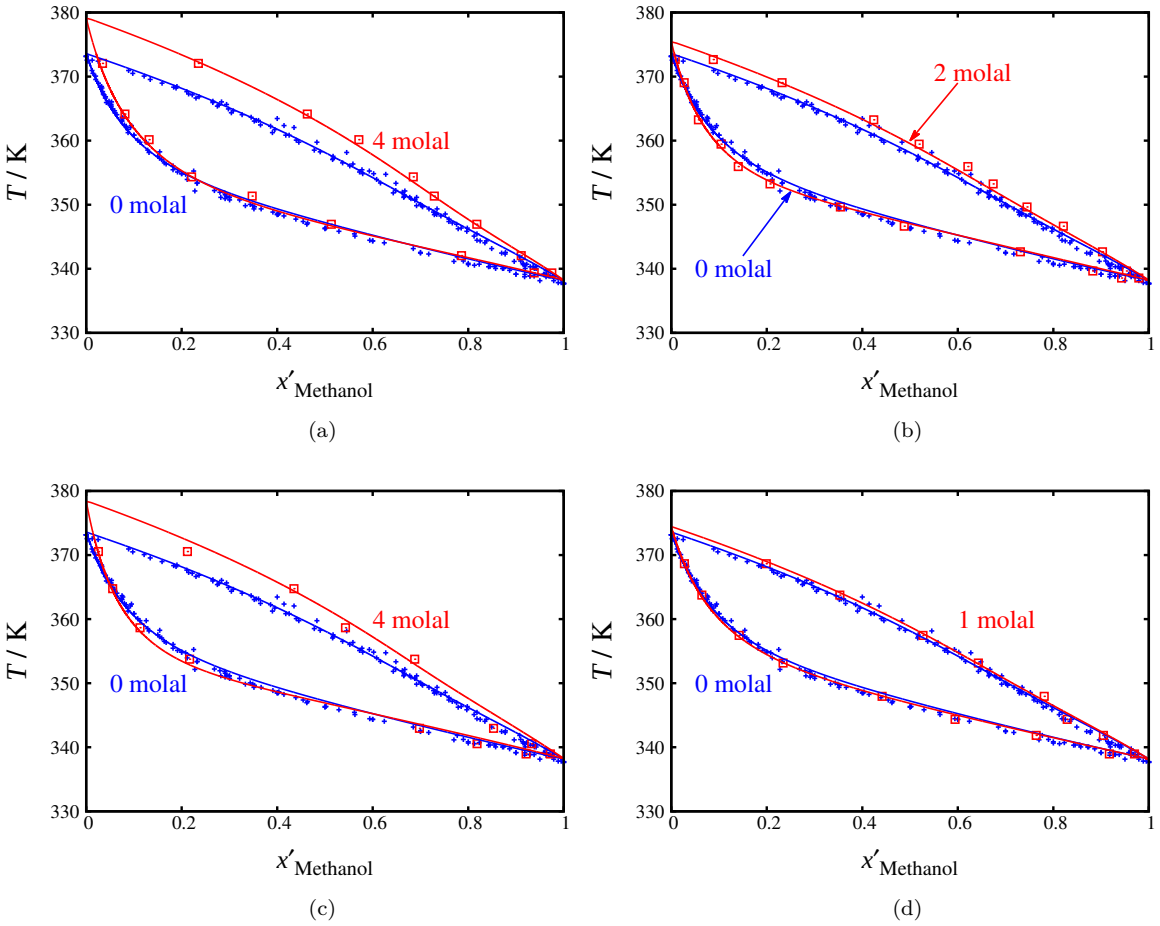

Figure 12: Isobaric representations of the vapour-liquid equilibria of water + methanol and water + salt + methanol at a pressure of $P = 1$ atm for different monovalent alkali-halide salts: (a) LiCl; (b) KCl; (c) NaBr; and (d) NaF. The symbols represent experimental data [173–179], and the continuous curves the description with the SAFT-VRE approach. Molalities are given with respect to water; the abscissa is the salt-free mole fraction, x'_{Methanol}, of methanol.

In Figure 13 the liquid-liquid equilibria of *n*-butan-1-ol + water + salt ternary systems at ambient conditions ($T = 298$ K and $P = 1$ bar) for three salts are presented. The estimated values of the butanol-ion dispersion energy parameter $\varepsilon_{\mathrm{Butanol-ion}}$ given in Table (11) are used for the SAFT-VRE calculations, and it can be seen that that the effect of the added salts on the liquid-liquid demixing of *n*-butan-1-ol + water mixtures is captured well. The addition of salt induces salting out of the alcohol, *i.e.*, a decrease of the *n*-butan-1-ol content in the water-rich phase, with the water content in the alcohol-rich phase also decreasing.

Table 11: The unlike dispersion energy parameter $\varepsilon_{\mathrm{Butanol-ion}}$ between the ion and *n*-butan-1-ol estimated from the *n*-butan-1-ol + water + salt liquid-liquid equilibrium data ambient conditions (T = 298 K and P = 1 bar) with the SAFT-VRE approach.

Ion	Na^+	K^+	Cl^-	Br^-
$(\varepsilon_{\mathrm{Butanol-ion}}/k_{\mathrm{B}})$ / K	274.0	424.0	151.0	418.0

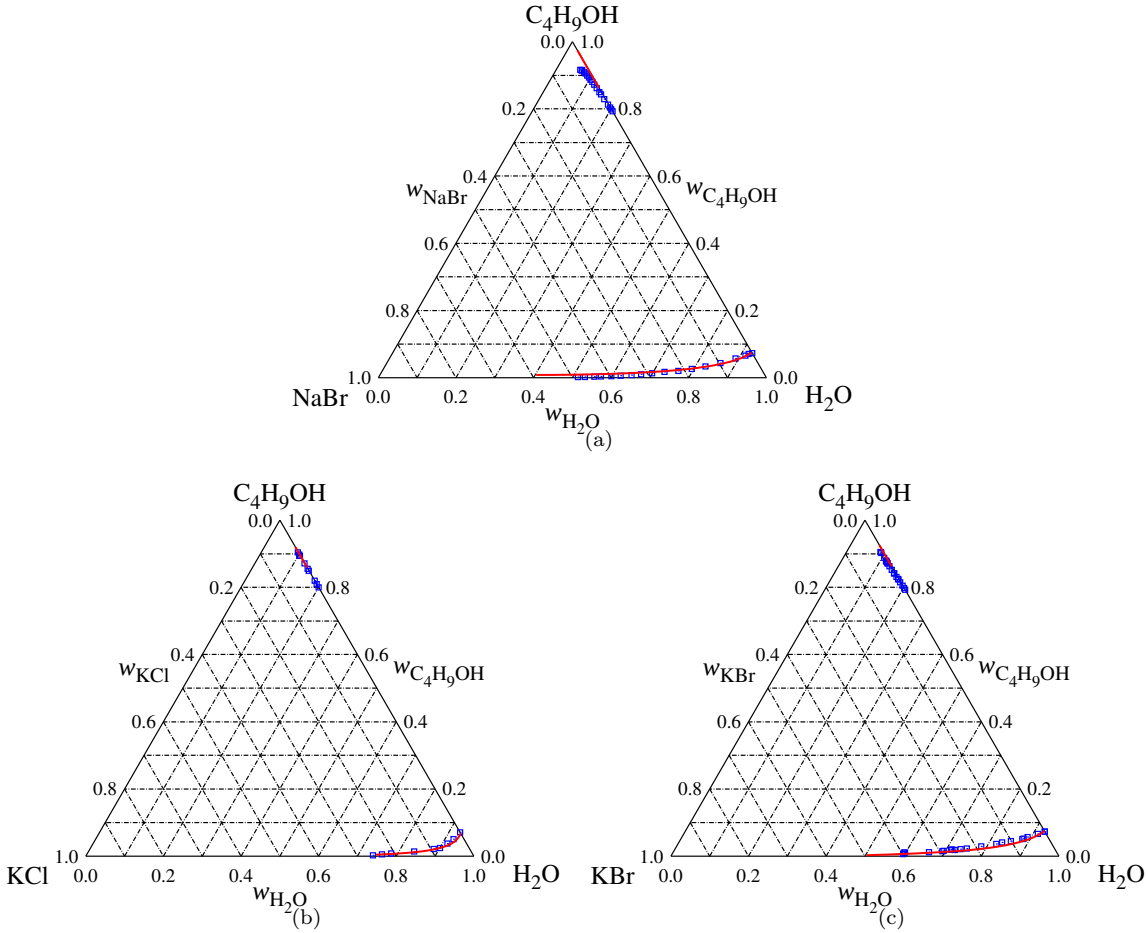

Figure 13: Isobaric-isothermal representation of the liquid-liquid equilibria for the water + salt + *n*-butan-1-ol ternary system at ambient condition (T= 298 K and $P = 1$ atm) for different monovalent alkali-halide salts: (a) NaBr; (b) KCl; and (c) KBr. The symbols represent the experimental data [180, 181] and the continuous curves the description with the SAFT-VRE approach; the axes represent the weight fractions of the different components.

5.2.5. Brine + carbon dioxide

As a consequence of increased interest in the injection of carbon dioxide in saline aquifers, the water + carbon dioxide + salt ternary system has been studied with a variety of methods (e.g., Hu *et al.* [182], Yan *et al.* [183] and Tong *et al.* [184]), and in view of the particular relevance to our current work we acknowledge a number of studies [121, 185–187] that have used SAFT approaches to treat these mixtures. Isothermal representations of the pressure-composition (P, x) fluid-phase behaviour for the solubility of carbon dioxide in pure water (the water-rich phase of the liquid-liquid boundary) and in 1 molal and 5 molal NaCl aqueous solutions at $T = 323$ K, obtained using our improved SAFT-VRE approach are presented in Figure 14. Additional experimental data are available for other conditions; here we show the description for only one representative temperature, to provide an indication of the predictive power of the approach. The water + carbon dioxide model is given in Table 3 and the water + ion models in Table 6. The effect of the addition of salt is obtained in a predictive way, as the unlike interaction parameters between the ions and carbon dioxide are obtained using equations (49), (50) and (54). The predictions of the SAFT-VRE approach are found to be in good agreement with the experimental data. It can be seen that the addition of salt results in a decrease of the solubility of carbon dioxide in water and that a greater degree of salting out is seen at higher salt concentration. A similar salting out trend is seen when other simple 1:1 salts are added to these aqueous solutions. The change in slope observed in the solubility of carbon dioxide in the aqueous solutions with increasing pressure is due to a change in fluid phase behaviour from vapour-liquid-like at low pressure to liquid-liquid-like at higher pressure, the change between the two types of phase coexistence is continuous as carbon dioxide is in a super critical state at the conditions shown. As can be seen, our approach reproduces this change in good agreement with the experimental data reported [188–195].

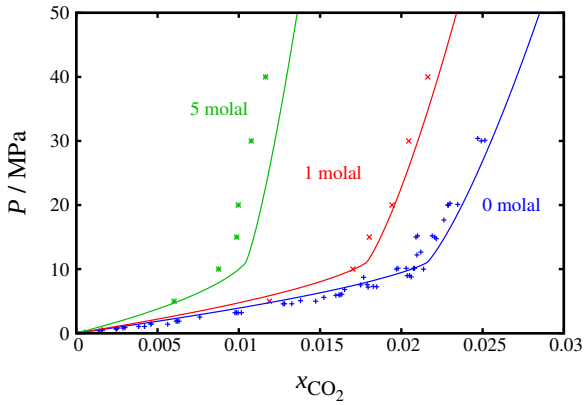

Figure 14: Pressure-composition constant temperature phase diagram of the water + carbon dioxide and Water + carbon dioxide + sodium chloride at $T = 323$ K; symbol represent experimental data [188–195] and the curves the description with the SAFT-VRE approach.

6. Conclusions

The extension of the SAFT-VR equation of state to electrolytes, referred to as SAFT-VRE, has been enhanced to make the approach more versatile and to improve its predictive capability. We have discussed how the incorporation of a Born term in the free-energy expression allows for solvation effects to be taken into account. Although only a semi-quantitative agreement is obtained, the calculated and experimental solvation energies of ions in water are seen to follow the same trends. A major advance in our new implementation of SAFT-VRE has been the introduction of a more-accurate and detailed representation of the dielectric that takes into account the temperature, density, and composition of the solvent. This empirical model allows for the description of a broad range of properties, some of which (such as the depression of freezing point, the osmotic coefficient, and the properties of multi-solvent solutions) had not been considered using previous implementations.

These developments allow for a rigorous solution of the conditions for fluid-phase-equilibrium, treating each phase in a consistent fashion and thereby improving the thermodynamic consistency of the approach; the liquid and vapour phases are treated on an equal footing allowing ions to be present in the vapour as well as the liquid phase; it is confirmed that the concentration of ions in the vapour phase is generally extremely low.

Intermolecular potential models have been developed for the group I alkali-metal and group VII halide ions in aqueous solution and in mixed water-alcohol solvents. As expected, these models provide an excellent representation of the properties used to estimate the specific parameters; these comprise the densities, vapour pressures, and mean-activity coefficients of aqueous solutions of single salts. The predictive capability of the theory has been demonstrated in describing other properties for both single and multisalt electrolyte solutions. The predictions of the osmotic coefficients and the depressions of freezing temperature of simple brines are very satisfactory considering that these data were not employed in the parameter estimation procedure. Additionally, the prediction of the densities and vapour pressures of multisalt brines are also found to be in very good agreement with the available experimental data.

The impact of the salt on the phase equilibria of mixed-solvent systems is governed by the partitioning of the ions between the two phases, which depends on the value of the dielectric constant in each phase. Accordingly, the effectiveness of our empirical description of the dielectric constant is demonstrated by the successful treatment of the challenging mixed-solvent brine systems. This is exemplified by calculations of the effect of added salt on the fluid-phase equilibria of the water + methanol and water + n-butan-1-ol binary solvent systems. Another important, and equally challenging system is that of carbon dioxide in brine; this mixture is currently very topical due to the increased interest in carbon storage in saline aquifers.

The salting-out of carbon dioxide from aqueous solution by sodium chloride is captured very well by our theory, notwithstanding that the calculations are undertaken in an entirely predictive manner.

In conclusion, the incorporation of an accurate density and temperature-dependent dielectric constant within the SAFT-VRE treatment enhances the versatility and predictive capability of the theory. It is interesting to note that, although the development of the intermolecular potential models for the interactions between the ions and the solvent was carried out using an approach based solely on descriptions of thermodynamic properties of the fluids, the parameters obtained for the ions follow physical trends in both the dispersion energies and in the sizes of the ions; the ionic diameters closely mirror the well-established ionic diameters of Shannon [125]. This is an important result, as the sensible physical trends obtained for the models provide confidence that models and theory may be used in predictive fashion beyond the systems that have been considered in this work.

Acknowledgements

We would like to acknowledge that the QCCSRC is funded jointly by Qatar Petroleum, Shell, and the Qatar Science & Technology Park. Further support from Engineering and Physical Sciences Research Council (EPSRC) of the United Kingdom (grants GR/T17595, GR/N35991, EP/E016340 and EP/J014958) to the Molecular Systems Engineering Group is gratefully acknowledged. We would also like to thank C. C. Pantelides and T. Lafitte for useful discussions.

[1] G. M. Wilson, J. Am. Chem. Soc. **86**, 127 (1964).
[2] H. Renon and J. M. Prausnitz, AIChE J. **14**, 135 (1968).
[3] D. S. Abrams and J. M. Prausnitz, AIChE J. **21**, 116 (1975).
[4] D.-Y. Peng and D. B. Robinson, Ind. Eng. Chem. Fundam. **15**, 59 (1976).
[5] O. Redlich and J. N. S. Kwong, Chem. Rev. **44**, 233 (1949).
[6] W. G. Chapman, K. E. Gubbins, G. Jackson, and M. Radosz, Fluid Phase Equilib. **52**, 31 (1989).
[7] W. G. Chapman, K. E. Gubbins, G. Jackson, and M. Radosz, Ind. Eng. Chem. Res. **29**, 1709 (1990).
[8] P. Debye and E. Hückel, Z. Phys. **24**, 185 (1923).
[9] P. Debye and E. Hückel, Z. Phys. **24**, 305 (1923).
[10] L. Blum, Mol. Phys. **30**, 1529 (1975).
[11] L. Blum and J. S. Høye, J. Phys. Chem. **81**, 1311 (1977).
[12] C. A. Haynes and J. Newman, Fluid Phase Equilib. **145**, 255 (1998).
[13] J. A. Myers, S. I. Sandler, and R. H. Wood, Ind. Eng. Chem. Res. **41**, 3282 (2002).
[14] G. M. Kontogeorgis and G. K. Folas, *Thermodynamic Models for Industrial Applications: From Classical and Advanced Mixing Rules to Association Theories* (Wiley, 2010).
[15] B. Maribo-Mogensen, G. M. Kontogeorgis, and K. Thomsen, Ind. Eng. Chem. Res. **51**, 5353 (2012).
[16] W. Fürst and H. Renon, AIChE J. **39**, 335 (1993).
[17] J. Schwartzentruber, H. Renon, and S. Watanasiri, Fluid Phase Equilib. **52**, 127 (1989).
[18] G. Soave, Chem. Eng. Sci. **27**, 1197 (1972).
[19] R. Macías-Salinas, J. R. Avendaño-Gómez, F. García-Sánchez, and M. Díaz-Cruz, Ind. Eng. Chem. Res. **52**, 8589 (2013).
[20] Y. Lin, K. Thomsen, and J.-C. de Hemptinne, AIChE J. **53**, 989 (2007).
[21] G. M. Kontogeorgis, E. C. Voutsas, I. V. Yakoumis, and D. P. Tassios, Ind. Eng. Chem. Res. **35**, 4310 (1996).
[22] M. S. Wertheim, J. Stat. Phys. **35**, 19 (1984).
[23] M. S. Wertheim, J. Stat. Phys. **35**, 35 (1984).
[24] M. S. Wertheim, J. Stat. Phys. **42**, 459 (1986).
[25] M. S. Wertheim, J. Stat. Phys. **42**, 477 (1986).
[26] J. Wu and J. M. Prausnitz, Ind. Eng. Chem. Res. **37**, 1634 (1998).
[27] R. Inchekel, J.-C. de Hemptinne, and W. Fürst, Fluid Phase Equilib. **271**, 19 (2008).
[28] G. Jin and M. D. Donohue, Ind. Eng. Chem. Res. **27**, 1073 (1988).
[29] P. Vimalchand and M. D. Donohue, Ind. Eng. Chem. Fundam. **24**, 246 (1985).
[30] P. Vimalchand, M. D. Donohue, and I. Celmins, in *Equations of State: Theories and Applications*, edited by K. C. Chao and J. Robinson, R. L. (American Chemical Society: Washington, D.C., 1986), pp. 297–313.
[31] I. G. Economou, C. J. Peters, and J. de Swaan Arons, J. Phys. Chem. **99**, 6182 (1995).
[32] G. D. Ikonomou and M. D. Donohue, AIChE. J. **32**, 1716 (1986).
[33] I. G. Economou and M. D. Donohue, Ind. Eng. Chem. Res. **31**, 2388 (1992).
[34] W.-B. Liu, Y.-G. Li, and J.-F. Lu, Fluid Phase Equilib. **160**, 595 (1999).
[35] D. Henderson, L. Blum, and A. Tani, ACS Symp. Series **300**, 281 (1986).
[36] A. Galindo, A. Gil-Villegas, G. Jackson, and A. N. Burgess, J. Phys. Chem. B **103**, 10272 (1999).
[37] A. Gil-Villegas, A. Galindo, and G. Jackson, Mol. Phys. **99**, 531 (2001).
[38] B. H. Patel, P. Paricaud, A. Galindo, and G. C. Maitland, Ind. Eng. Chem. Res. **42**, 3809 (2003).
[39] B. Behzadi, C. Ghotbi, and A. Galindo, Chem. Eng. Sci. **60**, 6607 (2005).
[40] B. Behzadi, B. H. Patel, A. Galindo, and C. Ghotbi, Fluid Phase Equilib. **236**, 241 (2005).
[41] L. F. Cameretti, G. Sadowski, and J. M. Mollerup, Ind. Eng. Chem. Res. **44**, 3355 (2005).

[42] C. Held, L. F. Cameretti, and G. Sadowski, Fluid Phase Equilib. **270**, 87 (2008).

[43] C. Held and G. Sadowski, Fluid Phase Equilib. **279**, 141 (2009).

[44] C. Held, A. Prinz, V. Wallmeyer, and G. Sadowski, Chem. Eng. Sci. **68**, 328 (2012).

[45] J. Gross and G. Sadowski, Fluid Phase Equilib. **168**, 183 (2000).

[46] J. Gross and G. Sadowski, Ind. Eng. Chem. Res. **40**, 1244 (2001).

[47] J. M. Walsh, H. J. R. Cuedes, and K. E. Gubbins, J. Phys. Chem. **96**, 10995 (1992).

[48] E. A. Müller and K. E. Gubbins, Ind. Eng. Chem. Res. **34**, 3662 (1995).

[49] T. Kraska and K. E. Gubbins, Ind. Eng. Chem. Res. **35**, 4727 (1996).

[50] K. Xu, Y. Li, and W. Liu, Fluid Phase Equilib. **142**, 55 (1998).

[51] E. K. Karakatsani, T. Spyriouni, and I. G. Economou, AIChE J. **51**, 2328 (2005).

[52] I. G. Economou, E. K. Karakatsani, G.-E. Logotheti, J. Ramos, and A. A. Vanin, Oil Gas Sci. Technol. **63**, 283 (2008).

[53] M. C. dos Ramos and C. McCabe, Fluid Phase Equilib. **290**, 137 (2010).

[54] Z. Liu, W. Wang, and Y. Li, Fluid Phase Equilib. **227**, 147 (2005).

[55] H. Zhao, M. C. dos Ramos, and C. McCabe, J. Chem. Phys. **126**, 244503 (2007).

[56] S. Herzog, J. Gross, and W. Arlt, Fluid Phase Equilib. **297**, 23 (2010).

[57] M. Kettler, I. Nezbeda, A. A. Chialvo, and P. T. Cummings, J. Phys. Chem. B **106**, 7537 (2002).

[58] R. J. Sadus, Mol. Phys. **89**, 1187 (1996).

[59] J. N. Israelachvili, *Intermolecular and surface forces* (Academic Press, 1992), 2nd ed.

[60] I. Nezbeda, Mol. Phys. **103**, 59 (2005).

[61] J. R. Loehe and M. D. Donohue, AIChE Journal **43**, 180 (1997).

[62] S. P. Tan, H. Adidharma, and M. Radosz, Ind. Eng. Chem. Res. **47**, 8063 (2008).

[63] G. N. I. Clark, A. J. Haslam, A. Galindo, and G. Jackson, Mol. Phys. **104**, 3561 (2006).

[64] M. C. dos Ramos, F. J. Blas, and A. Galindo, J. Phys. Chem. C **111**, 15924 (2007).

[65] M. C. dos Ramos, F. J. Blas, and A. Galindo, Fluid Phase Equilib. **261**, 359 (2007).

[66] A. J. Haslam, A. Galindo, and G. Jackson, Fluid Phase Equilib. **266**, 105 (2008).

[67] G. N. I. Clark, A. Galindo, G. Jackson, S. Rogers, and A. N. Burgess, Macromolecules **41**, 6582 (2008).

[68] N. Mac Dowell, F. Llovell, C. S. Adjiman, G. Jackson, and A. Galindo, Ind. Eng. Chem. Res. **49**, 1883 (2010).

[69] A. Georgiadis, F. Llovell, A. Bismarck, F. J. Blas, A. Galindo, G. C. Maitland, J. P. M. Trusler, and G. Jackson, J. Supercrit. Fluid. **55**, 743 (2010).

[70] N. Mac Dowell, F. E. Pereira, F. Llovell, F. J. Blas, C. S. Adjiman, G. Jackson, and A. Galindo, J. Phys. Chem. B **115**, 8155 (2011).

[71] J. M. Míguez, M. C. dos Ramos, M. M. Pineiro, and F. J. Blas, J. Phys. Chem. B **115**, 9604 (2011).

[72] E. Forte, J. P. M. Trusler, and A. Galindo, J. Phys. Chem. B **115**, 14591 (2011).

[73] V. Papaioannou, C. S. Adjiman, G. Jackson, and A. Galindo, Fluid Phase Equilib. **306**, 82 (2011).

[74] J. Rodriguez, N. Mac Dowell, F. Llovell, C. S. Adjiman, G. Jackson, and A. Galindo, Mol. Phys. **110**, 1325 (2012).

[75] S. Dufal, A. Galindo, G. Jackson, and A. J. Haslam, Mol. Phys. **110**, 1223 (2012).

[76] A. Gil-Villegas, A. Galindo, P. J. Whitehead, S. J. Mills, G. Jackson, and A. N. Burgess, J. Chem. Phys. **106**, 4168 (1997).

[77] A. Galindo, L. A. Davies, A. Gil-Villegas, and G. Jackson, Mol. Phys. **93**, 241 (1998).

[78] M. Born, Z. Phys. **1**, 45 (1920).

[79] P. Hünenberger and M. Reif, *Single ion solvation: Experimental and theoretical approaches to elusive thermodynamic quantities* (RSCPublishing, 2011).

[80] T. L. Hill, *Statistical Mechanics* (McGraw-Hill, 1956).

[81] M. Uematsu and E. U. Franck, J. Phys. Chem. Ref. Data **9**, 1291 (1980).

[82] D. P. Fernández, A. R. H. Goodwin, E. W. Lemmon, J. M. H. Levelt-Sengers, and R. C. Williams, J. Phys. Chem. Ref. Data **26**, 1125 (1997).

[83] A. H. Harvey and J. M. Prausnitz, J. Solution Chemistry **16**, 857 (1987).

[84] E. Waisman and J. L. Lebowitz, J. Chem. Phys. **52**, 4307 (1970).

[85] L. L. Lee, *Molecular thermodynamics of electrolyte solutions* (World Scientific Publishing Co. Pte. Ltd., 2008), 1st ed.

[86] K. Hiroike, Mol. Phys. **33**, 1195 (1977).

[87] V. Taghikhani, H. Modarress, M. K. Khoshkbarchi, and J. H. Vera, Fluid Phase Equilib. **167**, 161 (2000).

[88] L. Blum and Y. Rosenfeld, J. of Stat. Phys. **63**, 1177 (1991).

[89] J.-P. Simonin, L. Blum, and P. Turq, J. Phys. Chem. **100**, 7704 (1996).

[90] C. Grossmann and G. Maurer, Fluid Phase Equilib. **106**, 17 (1995).

[91] P. Wang, A. Anderko, R. D. Springer, and R. D. Young, J. Mol. Liq. **125**, 37 (2006).

[92] K. Levenberg, Q. Appl. Math. **2**, 164 (1944).

[93] D. Marquardt, J. Soc. Ind. Appl. Math. **11**, 431 (1963).

[94] M. K. Khoshkbarchi and J. H. Vera, AIChE Journal **42**, 249 (1996).

[95] F. Malatesta, Chem. Eng. Sci. **65**, 675 (2010).

[96] G. Wilczek-Vera and J. H. Vera, Fluid Phase Equilib. **312**, 79 (2011).

[97] G. Wilczek-Vera and J. H. Vera, Chem. Eng. Sci. **66**, 3782 (2011).

[98] E. Lladosa, A. Arce, G. Wilczek-Vera, and J. H. Vera, J. Chem. Thermo. **42**, 244 (2010).

[99] G. Wilczek-Vera and J. H. Vera, Fluid Phase Equilib. **236**, 96 (2005).

[100] G. Wilczek-Vera, E. Rodil, and J. H. Vera, Fluid Phase Equilib. **241**, 59 (2006).

[101] J. M. Prausnitz, R. N. Lichtenhaler, and E. G. de Azevedo, *Molecular thermodynamics of fluid-phase equilibria* (Prentice-Hall International Series, 1986), 3rd ed.

[102] M. L. Michelsen and J. M. Mollerup, *Thermodynamic models: Fundamentals & computational aspects* (Tie-Line, Denmark, 2007), 2nd ed.

[103] H. L. Friedman, J. Chem. Phys. **76**, 1092 (1982).

[104] P. T. Cummings, J. Chem. Phys. **85**, 6658 (1986).

[105] L. Blum and W. R. Fawcett, J. Phys. Chem. **97**, 7185 (1993).

[106] B. Maribo-Mogensen, G. M. Kontogeorgis, and K. Thomsen, J. Phys. Chem. B **117**, 3389 (2013).

[107] B. Maribo-Mogensen, G. M. Kontogeorgis, and K. Thomsen, J. Phys. Chem. B **117**, 10523 (2013).

[108] L. Onsager, J. Am. Chem. Soc. **38**, 1486 (1936).

[109] J. G. Kirkwood, J. Chem. Phys. **7**, 911 (1939).

[110] H. Fröhlich, *Theory of Dielectrics, Dielectric Constant and Dielectric Loss*, Monographs on the Physics and Chemistry of Materials (Oxford University, 1949).

[111] D. A. Fletcher, R. F. McMeeking, and D. Parkin, J. Chem. Inf. Comput. Sci. **36**, 746 (1996).

[112] T. Moriyoshi, T. Ishii, Y. Tamai, and M. Tado, J. Chem. Eng. Data **35**, 17 (1990).

[113] R. Whorton and E. S. Amis, Z. Phys. Chem. **17**, 300 (1958).

[114] M. N. García-Lisbona, A. Galindo, G. Jackson, and A. N. Burgess, Mol. Phys. **93**, 57 (1998).

[115] M. N. García-Lisbona, A. Galindo, G. Jackson, and A. N. Burgess, J. Am. Chem. Soc. **120**, 4191 (1998).

[116] J. P. Wolbach and S. I. Sandler, Ind. Eng. Chem. Res. **36**, 4041 (1997).

[117] B. Patel, Ph.D. thesis, University of London, Imperial College London, Department of Chemical Engineering and Chemical Technology (2004).

[118] A. Galindo and F. J. Blas, J. Phys. Chem. B **106**, 4503 (2002).

[119] G. H. Hudson and J. C. McCoubrey, Trans. Faraday Soc. **56**, 761 (1960).

[120] D. R. Lide, ed., *CRC Handbook of Chemistry and Physics* (CRC Press, 2005), 86th ed.

[121] J. Rozmus, J.-C. de Hemptinne, A. Galindo, S. Dufal, and P. Mougin, Ind. Eng. Chem. Res. **52**, 9979 (2013).

[122] V. M. M. Lobo, *Electrolyte solutions: literature data on thermodynamic and transport properties* (Department of Chemistry, University of Coimbra, 1984).

[123] D. A. Fletcher, R. F. M. Meeking, and D. Parkin, J. Chem. Inf. Comput. Sci. **36**, 746 (1996).

[124] L. Pauling, *The Nature of the Chemical Bond* (Cornell University Press, 1960), 3rd ed.

[125] R. D. Shannon, Acta Cryst. **A32**, 751 (1976).

[126] W. R. Fawcett, J. Phys. Chem. B **103**, 11181 (1999).

[127] G. E. Amado and L. H. Blanco, Fluid Phase Equilib. **226**, 261 (2004).

[128] C. W. Childs and R. F. Platford, Aust. J. Chem. **24**, 2487 (1971).

[129] H. F. Gibbard and G. Scatchard, J. Chem. Eng. Data **18**, 293 (1973).

[130] H. F. Gibbard, G. Scatchard, R. A. Rousseau, and J. L. Creek, J. Chem. Eng. Data **19**, 281 (1974).

[131] W. J. Hamer and Y. C. Wu, J. Phys. Chem. Ref. Data **1**, 1047 (1972).

[132] G. J. Janz and A. R. Gordon, J. Am. Chem. Soc. **65**, 218 (1943).

[133] G. C. Johnson and R. P. Smith, J. Am. Chem. Soc. **63**, 1351 (1941).

[134] T. Koennecke, V. Neck, T. Fanghaenel, and J. I. Kim, J. Solution Chem. **26**, 561 (1997).

[135] C. T. Liu and W. T. Lindsay, J. Solution Chem. **1**, 45 (1972).

[136] N. Miljevic, G. Dessauges, and W. A. van Hook, J. Solution Chem. **10** (1981).

[137] K. Nasirzadeh, D. Zimin, R. Neueder, and W. Kunz, J. Chem. Eng. Data **49**, 607 (2004).

[138] J. I. Partanen and P. O. Minkkinen, Acta Chem. Scand. **47**, 768 (1993).

[139] J. A. Rard and D. G. Archer, J. Chem. Eng. Data **40**, 170 (1995).

[140] R. P. Smith, J. Am. Chem. Soc. **61**, 500 (1939).

[141] R. P. Smith and D. S. Hirtle, J. Am. Chem. Soc. **61**, 1123 (1939).

[142] T. M. Davies, L. M. Duckett, J. F. Owen, C. S. Patterson, and R. Saleeby, J. Chem. Eng. Data **30**, 432 (1985).

[143] W. J. Hornibrook, G. J. Janz, and A. R. Gordon, J. Am. Chem. Soc. **64**, 513 (1942).

[144] L. L. Makarov, K. K. Evstropev, and Y. G. Vlasov, Zh. Fiz. Khim. **32**, 1618 (1958).

[145] S. Manohar, J. Ananthaswamy, and G. Atkinson, J. Chem. Soc. Faraday Trans. **88**, 991 (1992).

[146] C. S. Patterson, L. O. Gilpatrick, and B. A. Soldano, J. Chem. Soc. **0**, 2730 (1960).

[147] R. F. Platford, J. Chem. Eng. Data **18**, 215 (1973).

[148] D. G. Archer, J. Phys. Chem. Ref. Data **21**, 793 (1992).

[149] J. M. Prausnitz, R. N. Lichtenhaler, and E. G. de Azevedo, *Molecular thermodynamics of fluid-phase equilibria* (Prentice-Hall International Series, 1986), pp. 635 – 640, 2nd ed.

[150] S. I. Sandler, *Chemical and Engineering Thermodynamics* (John Wiley & Sons, 1999), pp. 575–577, 3rd ed.

[151] G. N. Lewis, M. Randall, K. S. Pitzer, and L. Brewer, *Thermodynamics* (McGraw-Hill, 1961), pp. 404–410, 2nd ed.

[152] W. R. Parrish and J. M. Prausnitz, Ind. Eng. Chem. Process Des. Dev. **11**, 26 (1972).

[153] H. F. Gibbard and A. Fawaz, J. Solution Chem. **3**, 745 (1974).

[154] H. Haghighi, A. Chapoy, and B. Tohidi, Ind. Eng. Chem. Res. **47**, 3983 (2008).

[155] G. F. Hüttig and W. Steudemann, Z. Phys. Chem. **126**, 105 (1927).

[156] F. Momicchioli, O. Devoto, G. Grandi, and G. Cocco, Ber. Bunsen-Ges. Phys, Chem. **74**, 59 (1970).

[157] H. Najibi, A. H. Mohammadi, and B. Tohidi, Ind. Eng. Chem. Res. **45**, 4441 (2006).

[158] A. D. C. Rivett, Z. Phys. Chem. **80**, 537 (1912).

[159] W. H. Rodebush, J. Am. Chem. Soc. **40**, 1204 (1918).

[160] G. Scatchard and S. S. Prentiss, J. Am. Chem. Soc. **55**, 4355 (1933).

[161] F. A. Schimmel, J. Chem. Eng. Data **5**, 519 (1960).

[162] H.-L. Hsu, Y.-C. Wu, and L.-S. Lee, J. Chem. Eng. Data **48**, 514 (2003).

[163] S. Iyoki, S. Iwasaki, and T. Uemura, J. Chem. Eng. Data **35**, 429 (1990).

[164] I. M. Shiah and H. C. Tseng, Fluid Phase Equilib. **124**, 235 (1996).

[165] D. E. Goldsack and A. A. Franchetto, Electrochim. Acta **22**, 1287 (1977).

[166] A. Kumar, Can. J. Chem. **63**, 3200 (1985).

[167] H. E. Wirth, J. Am. Chem. Soc. **59**, 2549 (1937).

[168] S. Al Ghafri, G. C. Maitland, and J. P. M. Trusler, J. Chem. Eng. Data **57**, 1288 (2012).

[169] P. Linstrom and W. Mallard, eds., *NIST Chemistry WebBook, NIST Standard Reference Database Number 69* (National Institute of Standards and Technology, Gaithersburg MD, 2013).

[170] B. Mock, L. B. Evans, and C.-C. Chen, AIChE J. **32**, 1655 (1986).

[171] I. Kikic, M. Fermeglia, and P. Rasmussen, Chem. Eng. Science **46**, 2775 (1991).

[172] C. Achard, C. G. Dussap, and J. B. Gros, Fluid Phase Equilib. **98**, 71 (1994).

[173] G. Bredig and R. Bayer, Z. Phys. Chem. **130**, 1 (1927).

[174] J. G. Dunlop, Master's thesis, Brooklyn Polytechnic Inst., NY (1948).

[175] H. E. Hughes and J. O. Maloney, Chem. Eng. Progr. **48**, 192 (1952).

[176] S. I. Green and R. E. Vener, Ind. Eng. Chem. Res. **47**, 103 (1955).

[177] J. Ocon and F. Rebolleda, J. An. R. Soc. Esp. Fis. Quim. Ser. B **54**, 525 (1958).

[178] R. S. Ramalho, F. M. Tiller, W. J. James, and D. W. Bunch, Ind. Eng. Chem. Res. **53**, 895 (1961).

[179] J. E. Boone, R. W. Rousseau, and E. M. Schoenborn, Advan. Chem. Ser. **155**, 36 (1976).

[180] Z. Li, Y. Tang, Y. Liu, and Y. Li, Fluid Phase Equilib. **103**, 143 (1995).

[181] T. A. Al-Sahhaf and E. Kapetanovic, J. Chem. Eng. Data **42**, 74 (1997).

[182] J. Hu, Z. Duan, C. Zhu, and I.-M. Chou, Chem. Geol. **238**, 249 (2007), ISSN 0009-2541.

[183] W. Yan, S. Huang, and E. H. Stenby, Int. J. Greenhouse Gas Control **5**, 1460 (2011).

[184] D. Tong, J. P. M. Trusler, and D. Vega-Maza, J. Chem. Eng. Data **58**, 2116 (2013).

[185] R. Sun and J. Dubessy, Geochim. Cosmochim. Acta **88**, 130 (2012), ISSN 0016-7037.

[186] X. Ji, S. P. Tan, and M. Radosz, Ind. Eng. Chem. Res. **44**, 8419 (2005).

[187] X. Ji and C. Zhu, Geochim. Cosmochim. Acta **91**, 40 (2012).

[188] S.-X. Hou, G. C. Maitland, and J. P. M. Trusler, J. Supercrit. Fluids **73**, 87 (2013).

[189] D. Koschel, J.-Y. Coxam, L. Rodier, and V. Majer, Fluid Phase Equilib. **247**, 107 (2006).

[190] W. Yan, S. Huang, and E. H. Stenby, Int. J. Greenhouse Gas Control **5**, 1460 (2011).

[191] A. Bamberger, G. Sieder, and G. Maurer, J. Supercrit. Fluids **17**, 97 (2000).

[192] R. Wiebe and V. L. Gaddy, J. Am. Chem. Soc. **63**, 475 (1941).

[193] R. D'Souza, J. R. Patrick, and A. S. Teja, Can. J. Chem. Eng. **66**, 319 (1988).

[194] Y. D. Zel'venskii, Zh. Fiz. Khim. **14**, 1250 (1937).

[195] C. R. Coan and A. D. King, J. Am. Chem. Soc. **93**, 1857 (1971).